RSC Sustainability

ROYAL SOCIETY OF CHEMISTRY

TUTORIAL REVIEW

View Article Online
View Journal | View Issue



Cite this: *RSC Sustainability*, 2024, **2**, 3235

# Sustainable brain-inspired electronics: digging into natural biomaterials for healthcare applications

João V. Paulin *[a] and Carlos C. B. Bufon *[bc]

Received 10th August 2024
Accepted 27th September 2024

DOI: 10.1039/d4su00459k

rsc.li/rscsus

With traditional medical technologies shifting towards a more personalized point-of-view, current semiconductor-based electronics may need high-performance computing capability for cognitive and adaptive functions based on unspecific, multi-input, and complex tasks. Hence, developing electronic devices with improved capabilities is of utmost interest. One option takes inspiration from the synapse functionalities of the human brain. Due to their scalability and low power consumption, memristors and electrolyte-gated transistors are ideal candidates for efficient brain-inspired applications. Additionally, combining these device architectures with natural biomaterials (environmentally benign, biodegradable, biocompatible, and mechanically conformable) represents a new horizon toward transient and implantable synaptic devices. Here, we advertised the advances in artificial synaptic systems based on natural biomaterials and how these devices can be integrated into sustainable and intelligent healthcare systems. Our comprehensive review formulates the steps necessary for the next generation of healthcare electronics to flourish.

**Sustainability spotlight**

The field of biomedical and bioelectronics is moving towards personalized approaches, which will require devices with enhanced cognitive and adaptive capabilities. Taking inspiration from the functions of the human brain, integrating natural biomaterials into platforms such as memristors and electrolyte-gated transistors holds great potential for sustainable and intelligent healthcare systems. Aligned with the United Nations' Sustainable Development Goals 3 (Good Health and Well-being), 9 (Industry, Innovation, and Infrastructure), and 12 (Responsible Consumption and Production), this review focuses on the advancements in artificial synaptic systems, utilizing environmentally friendly, biodegradable, biocompatible, and mechanically conformable natural biomaterials, while promoting responsible consumption and production practices.

## Introduction

The advances in electronics of the XX century have revolutionized the way we live. Electronics are the backbone in several emerging areas, such as 5G/6G communication, automation, industry 4.0, the internet of things, robotics, smart cities, virtual reality, *etc.*[1] Another field garnering a crescent evolution is intelligent and wearable electronics, which refers to portable and personal devices designed to offer continuous assistance and enhance humans' overall quality of life.[1–6]

A significant advantage of the wearable platform is its promise to shift the generic 'one-size well-suited to all' traditional medical technologies to a personalized version. Hence, the medical system becomes more cognitive and adaptive, focusing on unspecific, multi-input, and complex tasks (human–machine interaction, simultaneous local environment analysis, and decision-making) while being robust and flexible to support long-term wear.[2,4,7,8]

The core of such a personal electronic system relies on a high-performance computing capability. Nonetheless, conventional semiconductor-based electronics face limitations imposed by the von Neumann structure.[9–11] The "classical" von Neumann architecture consists of a central processing unit (CPU) responsible for deciding and executing an instruction, separated from the main memory, responsible for storing the instructions and data, Fig. 1a.[9] Although this separation can perform satisfactory structural tasks and has been responsible for all computing evolution in the past few decades, the high-volume data and the limited transmission speed between CPU and memory decrease the performance of the device when dealing with the complex multi-input of real-life tasks (the von Neumann bottleneck). Millions of interconnected processors could be a potential solution to this problem. However, each processor is still limited by its bottleneck, with a significant additional increase in processing power.[9] Take, for example, the Tianhe-2 supercomputer. It has an average of 20 MW of energy and power consumption of about 200 million kW h annually.[12]

[a]São Paulo State University (UNESP), School of Sciences, Department of Physics and Meteorology, Bauru, SP, Brazil. E-mail: jv.paulin@unesp.br
[b]São Paulo State University (UNESP), Institute of Geosciences and Exact Sciences (IGCE), Department of Physics, Rio Claro, SP, Brazil. E-mail: cesar.bof@unesp.br
[c]São Paulo State University (UNESP), Postgraduate Program in Materials Science and Technology (POSMAT), Bauru, SP, Brazil

To overcome the von Neumann bottleneck, the scientific community caught the eye of a natural supercomputer: the human brain. Compared to traditional computers, the human brain has the tremendous computational ability to perform 17 trillion multiple tasks per second, such as self-learning and cognitive functions (*e.g.*, abstract reasoning, linguistic comprehension, memory management, motor control, and visual imaging). It accomplishes this while consuming ~20 W of power in a small occupation volume (~1200 $cm^3$).[13–17] In comparison, IBM's TrueNorth chip, which utilizes 5.4 billion transistors and a silicon-based complementary metal-oxide-semiconductor circuit, emulates only about 1/1000th of the human brain's functionality, equivalent to 1 million neurons and 256 million configurable synapses.[12] This suggests the exceptional performance of biological machines.

The brain's high efficiency is attributed to the synaptic communication activity within its neural network, which simultaneously stores and processes information in the same synapse by adjusting the strength of the connection between adjacent neurons, Fig. 1b.[12,18,19] Accordingly, the bottleneck of conventional computers is eliminated due to the impossibility of distinguishing processing and memory — along with the advantages of being highly parallel, fault-tolerant, and, most importantly, highly efficient.[20–23] Hence, developing electronic devices with synaptic functions is of utmost interest for personalized healthcare. These devices can assist in automated diagnosis, predict treatments' benefits and side effects, enable personalized drug delivery, and support neuro-prosthetics. These challenges underpin two of the 14 grand challenges in the XXI century elucidated by the United States National Academy of Engineering:[7,24] *Advanced Health Informatics* and *Reverse-Engineer the Brain*.

In parallel to the health theme, the rapid growth in implementing better and improved devices for biosensing, monitoring, and therapeutic interventions undeniably contributes to a collateral rise in electronic waste (e-waste). E-waste is already a major social challenge today due to the potential to be hazardous to the environment and human health and the limited availability of strategic mineral resources.[25–28] In this case, Mother Nature could also inspire a solution. Abundant natural organic biomaterials, often environmentally benign, biodegradable, and biocompatible with mechanical softness, undeniably unveil a new horizon toward advanced sustainable medical electronics.[4,25,29–34] Furthermore, it is also a step toward

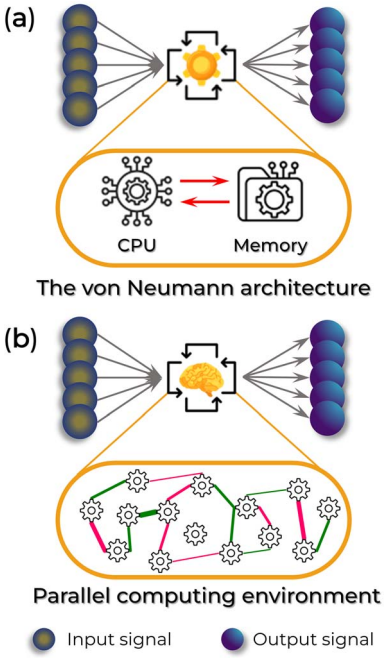


Fig. 1 Schematic comparison between the von Neumann (top) and neuromorphic (bottom) computing architectures. (a) Traditional computer structure. The red arrows indicate the von Neumann bottleneck. (b) A general brain-inspired architecture. The CPU and memory are co-localized across different neurons (represented by the black gearwheel) and synapses (green and pink lines with different thicknesses connecting the black gearwheels).

**João V. Paulin**

*Dr João V. Paulin is a researcher at São Paulo State University (UNESP) in the Department of Physics and Meteorology. He holds a PhD in Science and Technology of Materials from UNESP, where his doctoral thesis received the prestigious Thesis Award from the Brazilian Coordination for the Improvement of Higher Education Personnel (CAPES) as the best in the Materials field in Brazil in 2021. With expertise in Materials Science and Applied Physics, Dr Paulin's research interests lie at the intersection of biomaterials, sustainability, and organic (bio)electronics.*

**Carlos C. B. Bufon**

*Carlos C. B. Bufon received his bachelor's and master's degrees in physics, followed by a PhD from Heinrich-Heine Universität Düsseldorf, Germany. He has held numerous leadership roles, including as a group leader at the Leibniz Institute for Solid State and Materials Research in Dresden, Germany, a division head at the Brazilian Nanotechnology Laboratory, and Executive Director of Research and Innovation at Mackenzie Presbyterian Institute. He is an Alexander von Humboldt fellow and is currently a professor in the Physics Department at São Paulo State University in Rio Claro, Brazil. His research is centered on the physics of micro and nanodevices, with a particular emphasis on hybrid materials and systems.*

the United Nations's Sustainable Development Goals: 3 (Good Health and Well-being) and 12 (Responsible Consumption and Production).[35]

In this context, we present a comprehensive review of the rapid development of neuromorphic systems using natural biomaterials for sustainable biomedical and bioelectronics applications. The review is structured into background, applications, and conclusions. In the first section, we introduce the essential characteristics of both natural and artificial synapses and provide an overview of the primary features of these devices. Next, we explore recent advances in artificial synaptic devices based on biomaterials and discuss their integration into intelligent healthcare systems. Finally, we address key challenges and opportunities in the field. This timely review summarizes the latest advancements in biomaterial-based neuromorphic applications and offers insights into potential solutions for the next generation of sustainable biomedical electronics.

## Fundamental characteristics

### Biological synapse

A biological neural network can be formed by $10^{12}$ neurons connected by $10^{15}$ nanogap junctions (synaptic cleft), known as synapses, and, in most cases, it is between 10 and 70 nanometers wide (see Fig. 2a).[16,17,20,36,37] Neurons are electrically excitable cells consisting of soma, axons, and dendrites. They play a crucial role in producing, processing, and transmitting communication signals throughout the central nervous system (CNS), including the brain and spinal cord, and the peripheral nervous system (PNS), which encompasses sensory and motor organs and nerves.

The soma accumulates the input signals collected from the dendrites in the neural system. Above a certain threshold, the presynaptic neuron generates an action potential that propagates the valuable information towards the postsynaptic neuron through the axon and eventually transmits information to

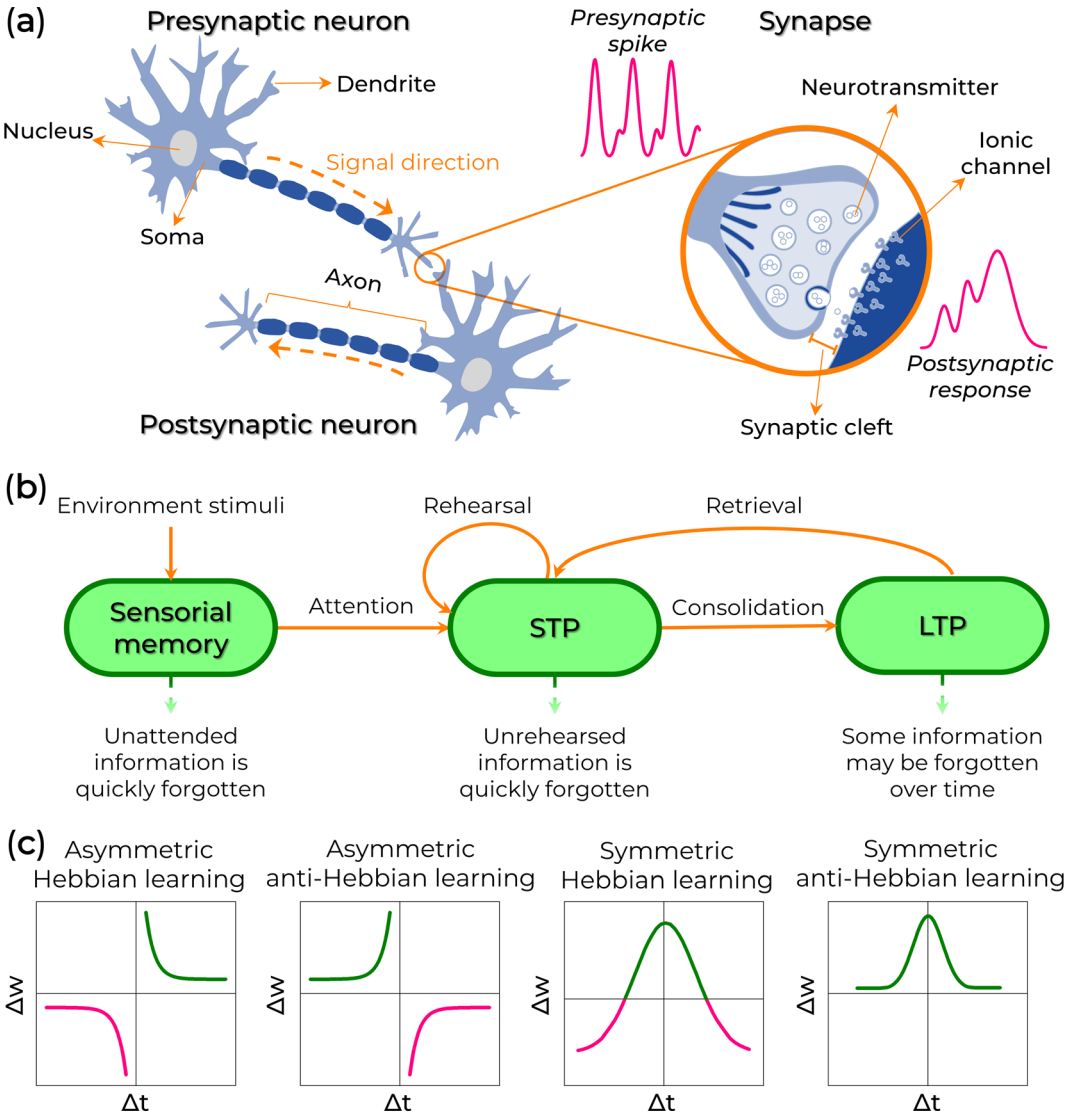


Fig. 2 (a) Illustration of a simple neuron network with a representation of the structure and component of a chemical synapse. (b) Schematic of a memory model based on the STP to LTP transition. (c) Examples of a few STDP rules.

organs.[14,16,20,36,38] These synaptic transmissions only consume 1–10 fJ of energy each.[17,39] The action potential can trigger chemical or electrical synapse signals between neurons, and the synaptic strength is defined as the synaptic weight ($w$).[36] Electrical synapses involve a relatively straightforward synaptic interaction between neurons, with minimal separation (around 3.5 nm synaptic cleft). They facilitate direct, rapid, and bidirectional transmission of electrical neural signals between neurons.[14,16,20] On the other hand, chemical synapses perform more complex signal transmissions. They can precisely regulate synaptic strength during learning, memory, and cognitive functions, including emotion, sensory signal transmission, and muscle activation.[14,16,20] They use neurotransmitters to transport neural signals between neurons with wider synaptic clefts (10 to 70 nm).[14,16,20] In this case, the presynaptic membranes release neurotransmitters dispersed across the synaptic cleft, bind to receptors (ionic channels), and are transmitted into the postsynaptic membrane (Fig. 2a). Changes in membrane potential can result in either an excitatory postsynaptic potential (EPSP) or an inhibitory postsynaptic potential (IPSP). In the case of an EPSP, the membrane is depolarized, allowing the neuron to respond to the stimulus by passing the signal to the next neuron. Conversely, with an IPSP, the membrane is hyperpolarized, suppressing signal transmission.

Synaptic plasticity is defined by the variation of $w$ over time. It is classified into short-term plasticity (temporary change of $w$, time scales of milliseconds to minutes) and long-term plasticity (long change of $w$, from minutes to the brain lifetime – LTP).[13,14,16,40,41] Short-term plasticity (STP) is the temporary storage of processed information, which can be discarded once it is no longer needed. This includes associative learning, pattern recognition, and sound localization functions.[13,14,40,42,43] In contrast, LTP is the permanent storage of processed information.[13,14,44,45] Therefore, the transition from STP to LTP represents a crucial and gradual neural process associated with human learning and memory (Fig. 2b).[13,14,16,45]

Changes in neuron topology, triggered by isolated, repeated, frequent, or infrequent stimulations, lead to the transition from STP to LTP.[45] Such a stimulus can be found in a potentiation or depression state. A potentiation state occurs when there's an increase in the postsynaptic potential, meaning that the same stimulus triggers a more significant number of action potentials. When action potentials become repetitive or frequent, the concentration of neurotransmitters near the postsynaptic membrane increases, leading to a corresponding growth in the number of ionic channels. This amplifies the volume of neurotransmitters that can be received, resulting in each subsequent postsynaptic potential being higher than the previous one for the same amount of chemical signal received by the postneuron (refer to Fig. 1b, thicker lines). This phenomenon is termed paired-pulse facilitation (PPF).[43,46,47] In contrast, a depression state arises when a more significant number of stimulations are required to elicit the same quantity of action potentials as previously observed (known as paired-pulse depression, PPD). In such instances, the concentration of ionic channels decreases, resulting in the postneuron receiving a weaker postsynaptic potential than in the preceding state (Fig. 1b, thin lines).

Following the Hebbian learning rule,[48] $w$ increases if a synapse continuously produces action potentials on its postsynaptic neuron. Hence, spike stimuli are an essential factor for learning. Therefore, the Hebbian rule can be treated as spike-timing-dependent plasticity (STDP) if the learning process considers the temporal order of synaptic spike stimulation. The STDP precisely modulates the connection strengths between neurons depending on the relative timing ($\Delta t$) between pre- and post-synaptic spikes.[15,49–52] The post-synaptic spike can be excitatory (resulting in excitatory post-synaptic current, EPSC) or inhibitory (leading to inhibitory post-synaptic current, IPSC). In this context, the absolute increase of $\Delta t$ can induce potentiation ($\Delta t > 0$, meaning a preneuron spikes before a postneuron) or depression ($\Delta t < 0$, indicating a postneuron spikes before a preneuron) responses to the same stimulus (Fig. 2c). Nonetheless, depression does not contribute to learning and memory. So, to alter the synaptic response mechanism, the stimulus can be weighed with different spike frequencies.[49,50,52,53] In this case, the adjustment of the EPSC average effect is known as spike-rate-dependent plasticity (SRDP). In addition, the order in which the spikes are fired and the dendritic position also affect the synapse type and plasticity.[49]

## Artificial synapse and synaptic behaviors

To surpass the von Neumann architecture, neuromorphic electronics must emulate the brain's performance in signal transmission and synaptic plasticity and achieve functionalities related to learning and memory.[21–23,54–57] The essence of this type of device is centered on memory behavior, making mobility (a crucial parameter for other device applications) a noncritical physical parameter. Applying the presynaptic signals to the neuromorphic system alters the conductance (or resistance) through mechanisms such as electron migration, ion migration, and phase transition. In response, the device generates EPSC or IPSC electrical responses related to synaptic plasticity. Synaptic behaviors like STP, LTP, PPF, STDP, and SRDP can be achieved depending on the presynaptic stimulation.[21–23,54]

Artificial synaptic devices can be categorized into (a) two-terminal (2-T) memristors, which operate based on electrochemical metallization, oxygen vacancies, charge-trapping, phase-change, and ion migration mechanisms, and (b) three-terminal (3-T) ion-migration electrolyte-gated transistors. Readers are referred to the provided references for a complete description of the other possibilities.[22,23,54,58,59]

## Memristors

The structure of a memristor consists of an active layer (ionic conductor or insulant) sandwiched between the top (TE) and bottom (BE) electrodes (Fig. 3a and b). These electrodes can be metals or a combination of a metal and a metallic oxide (Table 1). To be classified as a memristor, the device must exhibit a pinched hysteresis loop in its current–voltage ($I$–$V$) characteristics when subjected to a voltage sweep (Fig. 3c).[102] This signature response, a hallmark of memristive behavior, is

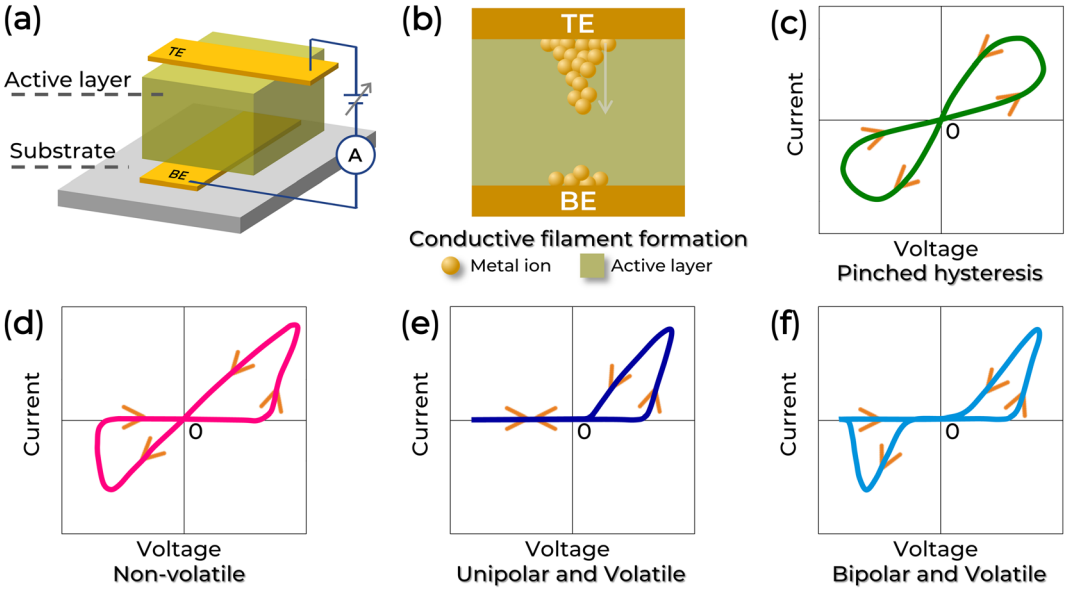


Fig. 3 (a) Schematic illustration of a 2-T memristor, (b) its electrochemical metallization operation mode, and (c) a typical pinched hysteresis loop from a voltage sweep curve. (d–f) Representation of different IV curves for various memristive mechanisms.

documented across various *I–V* profiles. These profiles encompass both volatile and non-volatile, as well as unipolar and bipolar memristive devices (Fig. 3d and e).[102,103]

Volatile memristors are characterized by their inability to retain stored information once the power supply is removed, making them suitable for applications requiring temporary data storage.[102,104] In contrast, non-volatile memristors preserve information without power, a crucial feature for long-term data retention and non-volatile memory applications.[22,102,104] Memristive devices can be classified based on their response to voltage polarity. Unipolar devices switch states under a single polarity voltage, while bipolar devices necessitate alternating polarities to transition between the high-resistance state (HRS) and low-resistance state (LRS).[22,102,103]

A memristor operating on the electrochemical metallization (ECM) principle is governed by the migration and redox of metal ions under an applied bias.[23,54,105] When a voltage bias is applied to the top electrode, oxidation reactions occur at its interface, forming metal cations that diffuse into the dielectric layer under the influence of the electric field. During diffusion, these cations can interact with electrons or anions and undergo reduction reactions, forming conductive particles. With sufficient stimulus, these conductive particles can evolve into a conductive filament between the cathode (TE) and the anode (BE), Fig. 3b.[23,54,105] The current rapidly increases once the conductive filament is formed, signifying the ON state.

Additionally, the device's conductivity can increase with a continuous voltage application and modulation, thickening the filament.[23,54,105] The ON state corresponds to LRS. However, the metallic filament is unstable and can rupture by ionization, Joule heating, spontaneous diffusion, or degradation over time. In this situation, the current decreases, causing the device to switch to HRS or OFF state.

Expanding on this, a memristor operating based on oxygen vacancies relies on changes at the interface between a metal electrode and a metal oxide semiconductor.[106–108] The metal oxide is initially in HRS and is sustained by an energy barrier. When a voltage is applied, oxygen vacancies within the metal oxide move due to the electric field, reducing the Schottky or tunnel barrier. This reduction can lead to the formation of conductive filaments, transitioning the device to LRS. When the voltage is reversed, the oxygen vacancies return to their original positions, or the conductive filaments break, restoring the energy barrier and reverting the metal oxide to the HRS.

Similarly, charge-trapping-based memory exploits the phenomenon where charges fill traps in insulating layers. Initially, electron injection follows ohmic conduction, with current proportional to the applied voltage. As more charges are injected and occupy these traps, the conduction mechanism shifts to a space-charge-limited current (SCLC) regime, where injected carriers exceed thermally generated ones.[109–111] In cases where the metal electrode forms an ohmic contact with the insulating layer without any traps filled, the current is governed by space charge. Introducing charge-trapping nanoparticles into the insulating layer enables voltage-induced trapping, transitioning from ohmic to SCLC conduction.[110,111] This mechanism is fundamental to memristors' long-term memory and learning/forgetting capabilities.

Phase-change memory leverages the reversible transition between amorphous and crystalline states induced by Joule heating.[83,112,113] The amorphous state corresponds to HRS, whereas the crystalline state represents LRS. Applying current raises the material's temperature to its crystallization point, switching it to the LRS in a process known as the “set” operation. Conversely, raising the temperature to the melting point and rapidly cooling it returns the material to its amorphous state, the “reset” operation, thus reverting to the HRS. Repeated

Table 1 Outline of 2-T natural biomaterial-based artificial synapses[a]

| Mechanism | Substrate | Bottom electrode | Top electrode | Dielectric | Active area ($mm^2$) | $d$ (nm) | Energy (or power) consumption | Plasticity | Spike plasticity | Application | Ref. |
|---|---|---|---|---|---|---|---|---|---|---|---|
| IM | PEN | ITO | Al | Agarose@AuNP | 0.80 | — | 64.4 pJ | + | + | Pattern recognition | 60 |
| ECM + IM | PET | ITO | Ag | CuO-doped albumen | 30 m | 300 | 4.9 μJ | + | + | Pattern recognition | 61 |
| ECM | Glass | ITO | Ag/Al | Albumen | — | 600 | — | + | – | — | 62 |
| ECM | PET | ITO | W | Albumen | 5 m | 300 | 20 nJ | + | + | — | 63 |
| ECM | Glass | ITO | Al | Albumen@MWCNT | — | — | — | + | – | — | 64 |
| ICT | Glass | ITO | Al | PMMA/ Albumen@GQD/PMMA | — | 91 | — | + | + | Pavlov | 65 |
| ECM | $Si/SiO_2$ | Ti/Pt | Ag | ι-Carrageenan | 7.9 m | 100 | — | + | – | Pattern recognition | 66 |
| ECM + IM | Glass | FTO | Ag | $AgNO_3$-doped ι-carrageenan | — | — | 3.6 μW | + | + | Pattern recognition | 67 |
| ECM | Glass & PET | ITO | Ag | Ag-doped carrageenan | 0.8 | 80 | — | + | + | — | 68 |
| ECM | Glass | FTO | Ag | Ag-doped cellulose nanocrystal | 0.1 m | 4.4k | — | + | + | — | 69 |
| ECM | Glass | FTO | Ag | Cellulose@$Ti_3C_2T_x$ MXene | 3.14 | ~92k | — | – | + | — | 70 |
| OV | Glass | ITO | Al | GO : chitosan | — | — | — | + | – | Pavlov | 71 |
| OV | Glass | FTO | Ag | RGO : chitosan | 9.3 m | — | — | + | – | — | 72 |
| ECM | PEN | ITO/Ti/Pt | Ti | SWCNT/chitosan | 1.3 m | 80 | — | + | + | — | 73 |
| ECM | $Si/SiO_2$ | Ti/Pt | Ti | Chitosan | 30 m | 150 | — | + | – | — | 74 |
| IM | PET | ITO | Mg | Collagen | 10 m | 80 | 0.3 μJ 28 μW | + | + | — | 75 |
| ECM | $SiO_2$ | Pt/Ti | Cu/Ti | $Cu^{2+}$-doped DNA | — | 20 | — | + | + | Pattern recognition | 76 |
| ECM | — | ITO | Ag | DNA | — | 70 | — | + | + | — | 77 |
| ECM | Glass | ITO | Ag | Honey | 250 m | 2.2k | — | + | + | — | 78 |
| ECM | Glass | $Cu_xO/Cu$ | Cu | Honey | 6.3 m | 2.5k | — | + | + | Transient | 79 |
| ECM | Glass | ITO | Al | Honey | — | — | — | + | – | — | 80 |
| ECM + IM | $PHB_{92}$/ $PHV_8$ | MgO/W | Mg | Hyaluronic acid | — | — | — | + | – | Transient & implantable | 81 |
| ECM | PEN | ITO | Ag | Keratin | 7.9 m | 25 | — | + | + | Pattern recognition | 82 |
| ECM + PC | PET | ITO | Au | Lignin | 7.9 m | 180 | 0.5 μJ 49 μW | + | + | — | 83 |
| IM + OV | Glass | ITO | Al | Lactalbumin/Lotus root | — | 150 | — | + | + | — | 84 |
| ECM | $Si/SiO_2$ | Pt | Ti | Milk/$Ta_2O_5$ | — | 140 | — | + | + | Pattern recognition | 85 |
| ECM | $Si/SiO_2$ | Ag | Ag | Protein-nanowire | 6.4 m | 1k | — | + | + | — | 86 |
| ECM | $Si/SiO_2$ | W | Mg | Silibinin | — | — | 500 nJ | + | + | — | 87 |
| CF@OV | Glass | ITO | Al | Au-doped silk | — | 63 | — | + | + | — | 88 |
| ECM | Glass | ITO | Ag | Ag-nanoclusters@Silk fibroin | 6.4 m | 30 | 7 μW | + | + | — | 89 |
| ECM | $Si/SiO_2$ | Ni/Au | Ag | Ag-doped silk | 6.4 m | — | — | + | – | — | 90 |
| ECM | Glass | ITO | Ag | Keratin@Au-doped silk | 6.4 m | 80 | — | + | + | Transient & implantable | 91 |

Table 1 (*Contd.*)

| Mechanism | Substrate | Bottom electrode | Top electrode | Dielectric | Active area ($mm^2$) | $d$ (nm) | Energy (or power) consumption | Plasticity | Spike plasticity | Application | Ref. |
|---|---|---|---|---|---|---|---|---|---|---|---|
| ECM | — | ITO | Ag | Silk fibroin | 6.4 m | 25 | — | + | + | Pattern recognition | 92 |
| ECM | PDMS | Cu | Cu | Silk fibroin | 0.8 | 0.5M | — | + | + | Wearable | 93 |
| CF@OV | Glass | ITO | Al | Silk fibroin-GO | 79 | — | — | + | + | Pattern recognition | 94 |
| ECM | Glass | ITO | Al | Soybean@AuNP | 0.8 | 23 | — | + | + | — | 95 |
| OV | Glass | ITO | Al | Soybean@MWCNT | 0.80 | 114 | — | + | − | — | 96 |
| C-rF | Glass | ITO | Pt | Amylum | — | 153 | — | + | + | — | 97 |
| IM | Glass | ITO | Al | Starch@AuNP | — | — | 0.12 W | + | − | — | 98 |
| ECM | Ti | ITO | Ag | Starch : PVDF | 3.0 | 600 | — | + | + | Pattern recognition | 99 |
| IM | Glass | FTO | W | Trypsin | — | — | — | − | + | — | 100 |
| ECM | Glass | ITO | Al | Zein | 1.6 m | — | 80 nJ | − | + | Pattern recognition | 101 |

[a] Minus sign (−, not inferred); plus sign (+, inferred); ECM (electrochemical metallization); PC (phase-change); IM (ion migration); OV (oxygen vacancies); ICT (interfacial charge trap); CF@OV (conductive filament composed of oxygen vacancies); C-rF (carbon-rich filament); PDMS (polydimethylsiloxane); PET (polyethylene terephthalate); PEN (polyethylene naphthalate); $PHB_{92}$/$PHV_8$ (polyhydroxybutyrate/polyhydroxyvalerate); ITO (indium tin oxide); FTO (fluorine-doped tin oxide); PVDF (polyvinylidene fluoride).

application of short, small voltage pulses generates heat that creates unstable conductive filaments, which can easily break, showing short-term memory characteristics.[83] Continuous voltage pulses stabilize these filaments, resulting in long-term memory properties.[83]

Lastly, ion migration mechanisms exploit the movement of ions within the membrane's structure under an electric field.[23,75,98,114] The low activation energy required for ion migration induces hysteresis in *I–V* sweeps, utilized in various memory devices and artificial synapses. The migration of ions in response to a voltage pulse can change the device's resistance, demonstrating synaptic behavior. The structure and composition of the memristor significantly influence its operational mechanism and synaptic characteristics. Devices with optimal ion migration properties can achieve low driving voltages and reduced energy consumption per synaptic event, enhancing their efficiency and performance.[114]

### Electrolyte-gated transistor

An electrolyte-gated transistor (EGT) consists of source (S) and drain (D) electrodes in contact with a thin semiconductor layer, which is separated from the gate (G) electrode by a gating dielectric. This material is electronically insulating but ionically conductive (Fig. 4a). The S, D, and G electrodes can be made of metals, metal oxides, or organic compounds (Table 2). Applying a gate voltage causes ion migration at the electrode/electrolyte and electrolyte/channel interfaces, leading to the accumulation or depletion of charge carriers in the conducting path.[22,23,54,149] The key concept behind electrolyte gating is the electric-double layer, with a capacitance typically on the order of $\mu F\ cm^{-2}$. This high capacitance allows the EGT to operate at relatively low gate voltages and achieve large charge carrier densities in the conducting path. Additionally, the electrolyte capacitance is virtually independent of the layer thickness, enabling thick electrolyte layers for low-voltage operation.[22,23,54,149]

Regarding operating mechanisms, EGTs can function through electrical double-layer (EDL) and electrochemical (EC) mechanisms. In the EDL case, the semiconductor's conducting path is impermeable to the electrolyte ions, resulting in electrostatic doping (Fig. 4b left and c). Conversely, in the EC case, the semiconductor allows the ions to enter the film, leading to a reversible electrochemical doping/de-doping process (Fig. 4b right and d).[22,23,54,149]

As transistors, their electrical responses are characterized by the transfer ($I_D$–$V_G$) and output ($I_D$–$V_D$) curves, where $I_D$ is the drain current, $V_D$ is the drain voltage, and $V_G$ is the gate voltage. The left panels of Fig. 4c and d display the typical transfer characteristics of EDL and EC transistors, respectively, while the middle panels show the output characteristics.

The intrinsic amplification, known as transconductance ($g_M$), can be obtained from the slope of the linear region of the transfer characteristic ($I_D$–$V_G$) and is indicated by the dashed orange lines in Fig. 4c and d. The $g_M$ value depends on the EGT architecture (including the channel semiconductor and geometry), the ionic species in the electrolyte, and bias conditions.[149]

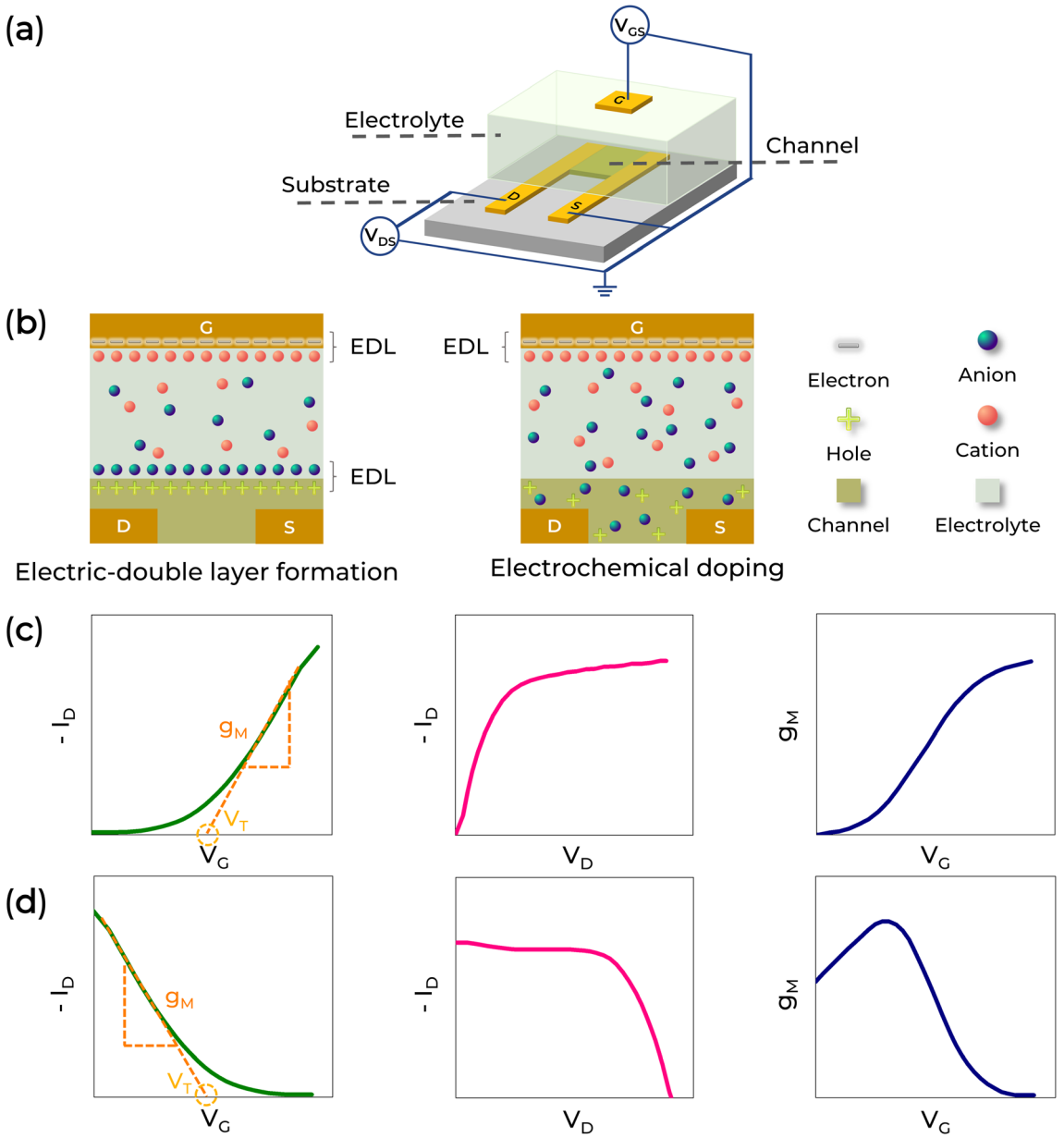


Fig. 4 (a) Schematic illustration of a 3-T electrolyte-gated transistor synaptic devices operating in (b) EDL and electrochemical doping modes with (c and d) their electrical characteristics. In (c and d), the transfer characteristic with transconductance $g_M$ and threshold voltage $V_T$ (left), the output characteristic (middle), and a typical $g_M$ *vs.* $V_G$ (right) are represented. The maximum of $g_M$ depends on $V_G$ and $V_D$.

A typical $g_M$ curve as a function of $V_G$ is shown in the right panels of Fig. 4c (EDL transistors) and 4d (EC transistors). Additionally, the intersection of the linear region of the transfer characteristic with the $V_G$ axis represents the threshold voltage ($V_T$). This threshold voltage can indicate fixed charges into the polymer (or molecular layers), the electrolyte's bulk ionic concentration, the gate work function, and the semiconductor's Fermi level.[149]

To maintain coherence between the operating mechanisms and their applications in neuromorphic systems, one needs to consider how these underlying principles impact device performance and scalability. Both EDL and EC mechanisms influence key parameters such as stability, energy efficiency, and processing techniques, which are necessary conditions for large-area applications and consistent functionality in complex systems.[150,151] Understanding these mechanisms lays the groundwork for exploring the broader implications of material choices and device architecture on the practical deployment of EGTs in neuromorphic computing.

The stability of EGT's performance is significantly influenced by the choice of electrolyte and the materials used in the device's architecture. Natural electrolytes, such as chitosan and maltose, have been shown to provide stable operation due to their favorable ionic conductivity. A well-chosen electrolyte can significantly improve stability by minimizing ion migration and leakage currents, which are known to degrade long-term

Table 2 Outline of 3-T natural biomaterial-based artificial synapses[a]

| Mechanism | Substrate | Gate | Source & drain | Dielectric/electrolyte | Active | Structure | W/L | Energy (or power) consumption | Plasticity | Spike plasticity | Application | Ref. |
|---|---|---|---|---|---|---|---|---|---|---|---|---|
| IM | Glass | ITO | ITO | Albumen | ITO | P | 13 | — | + | – | — | 115 |
| IM | Glass | ITO or IZO | IZO | Albumen | IZO | P & Co–P | 13 | — | + | + | — | 116 |
| IM | Glass | ITO | ITO | Casein | IGZO | P | 5 | — | + | + | Pattern recognition | 117 |
| IM | Cellulose | Au | Au | Cellulose | C8-BTBT | Co–P | 30 | 0.2 nJ | + | + | — | 118 |
| IM | Cellulose | Au | Au | Cellulose | Chlorophyll@ PDPP4T | P | 20 | — | + | – | Pattern recognition | 119 |
| IM | Glass or plastic | ITO | ITO | Cellulose | ITO | P | 12.5 | — | + | + | Anxiety disorder emulation & transient | 120 |
| IM | Glass | ITO | Al | Cellulose/PVA | IGZO | P | 1 & 1.5 | 5 pJ | + | + | Pattern recognition | 121 |
| ICT | Glass | ITO[b] | Au | Cellulose/PEG/NaCl | PBTTT-C14 or ITIC-F | P | 0.1 | — | + | + | Pavlovian & pattern recognition | 122 |
| IM | PI tape | ITO | ITO | Chitosan | ITO | P | 13 | 4.3 nJ 0.4 μW | + | + | Pavlovian | 123 |
| IM | Si | ITO | ITO | Gelatin@Chitosan | ITO | P | — | — | + | + | High-pass filter & pavlovian | 124 |
| IM | $Si/SiO_2$ | Ni | Ni | Chitosan | $MoS_2$ | Co–P | — | 5 pJ | + | – | — | 125 |
| IM | Paper | IZO | IZO | Chitosan | IZO | Co–P | 13 | 0.2 nJ 24 nW | + | + | — | 126 |
| IM | Chitosan | IZO | IZO | Chitosan | IZO | Co–P | 13 | 3.9 pJ | + | – | Logic | 127 |
| IM | $p\text{-}Si/SiO_2$ | Al | $N^+$-type | Chitosan/$Ta_2O_5$ | Si-nanowire | P | 1.3 | 2.7 to ∼200 nJ | + | + | Pattern recognition | 128 |
| IM | Polyimide | ITO | ITO | Chitosan/$Ta_2O_5$ | IGZO-nanowire | P | — | — | + | + | Pattern recognition | 129 |
| ICT | Si | SWCNT | Cr/Au | $SiO_2$ | Chlorophyll | P | — | 17.5 fJ | + | + | Transient & optical storage | 130 |
| ICT | Si | Si | Au | $SiO_2$ | Chlorophyll @PDPP4T | P | 60 | 0.5 fJ | + | – | Image processing | 131 |
| IM | None | Au | Au | Dextran | DNTT | P | — | — | + | + | Transient | 132 |
| IM | Si | Au | Au | Dextran T500 | DNTT | P | — | — | + | – | — | 133 |
| IM | Si | GaIn | Au | Gelatin | PEDOT : PSS | P | — | — | + | + | — | 134 |
| IM | p-Si (100) | Ag | Au | Keratin | PCDTPT | P | ∼5 | — | + | + | Transient | 135 |
| IM | PET | MAE | ITO | — | ITO | P | ∼6.7 | — | + | – | — | 136 |
| IM | — | — | ITO | Lactose-citrate acid | $In_2O_3$ | P | — | — | + | + | Pattern recognition | 137 |
| IM | Glass | ITO | ITO | Milk | IGZO | Co–P | 12.5 | — | + | + | — | 138 |
| IM | Si | Au | Au | Pectin | DNTT | P | — | — | + | + | Transient & implantable | 139 |
| ICT | Si/OTS | PEDOT : PSS | Au | Pectin | DNTT | P | — | — | + | + | Retina-inspired system | 140 |
| IM | Glass | ITO | ITO | Pectin | ITO | P | 12.5 | — | + | + | — | 141 |
| ICT | Glass or SIBS | Au | Au | PDA | PEDOT : PSS | Co–P | — | — | + | + | — | 142 |

Table 2 (*Contd.*)

| Mechanism | Substrate | Gate | Source & drain | Dielectric/electrolyte | Active | Structure | W/L | Energy (or power) consumption | Plasticity | Spike plasticity | Application | Ref. |
|---|---|---|---|---|---|---|---|---|---|---|---|---|
| — | Si/OTS | PEDOT : PSS | Au | Pullulan | C8-BTBT | P | — | — | + | – | — | 143 |
| ICT | $Si/SiO_2$ | Si | Au | $SiO_2$ | Silk@CD/ Pentacene | P | 50 | — | + | + | Pattern recognition | 144 |
| IM | Sodium alginate | AZO | AZO | Sodium alginate | AZO | Co–P | 7 | 2.8 nJ 0.3 μW | + | + | — | 145 |
| IM | $Si/SiO_2$ | ITO | ITO | Sodium alginate | ITO | Co–P | — | — | + | + | Pain-perception emulation | 146 |
| IM | Paper | ITO | ITO | Starch | IGZO | Co–P | 12.5 | — | + | + | Pattern recognition | 147 |
| ICT | Glass | ITO | ITO | Starch | ITO | P | | — | + | + | Transient | 148 |

[a] P (planar geometry); Co–P (co-planar geometry); MAE (maltose–ascorbic acid electrolyte); OTS (octadecyltrichlorosilane); SIBS (poly(styrene-*block*-isobutylene-*block*-styrene)); SWCNT (single-walled carbon nanotubes); IZO (indium–zinc-oxide); AZO (indium-free Al-doped zinc oxide); IGZO (indium–gallium–zinc oxide); C8-BTBT (2,7-dioctyl[1]-benzothieno[3,2-*b*]-[1]-benzothiophene); DNTT (dinaphtho[2,3-b:20,30-f]thieno[3,2-*b*]-thiophene); PDPP4T (poly{[2,5-bis(2-hexyldecyl)-3,6-diketopyrrolopyrrole-1,4-diyl]-*alt*-[2,2′-(3,3′-didodecyl-(2,2′;5′,2″;5″,2‴-quaterthiophene)]}); PBTTT-C14 (poly[2,5-bis(3-tetradecylthiophene-2-yl)-thieno[3,2-*b*]thiophene}); ITIC-F (9-bis(2-methylene-((3-(1,1-dicyanomethylene)-6,7-difluoro)-indanone))-5,5,11,11-tetrakis(4-hexylphenyl)-dithieno[2,3-d:2′,3′-d′]-*s*-indaceno[1,2-*b*:5,6-*b*′]dithiophene); $MoS_2$ (molybdenum disulfide); PCDTPT (poly[4-(4,4-dihexadecyl-4*h*-cyclopenta[1,2-*b*:5,4-*b*]dithiophen-2-yl)-alt[1,2,5]thiadiazolo[3,4-*c*]-pyridine]); PEDOT : PSS (poli(3,4-etilenodioxitiofeno) : poli(estireno sulfonado)); CD (carbon dots); PDA (polydopamine). [b] Presumably, although not stated in the paper.

performance. For instance, chitosan-gated transistors exhibit stable ionic/electronic coupling at the interface between the electrolyte and the channel,[152] while maltose-based electrolyte gates enable precise conductance adjustments, enhancing the devices' ability to support the kind of synaptic plasticity essential for neuromorphic systems.[136]

Scalability is a key advantage of EGTs. Solution-processing techniques used in the fabrication of these devices allow for flexible and large-scale production without sacrificing performance.[120,153] This scalability is especially important for integrating EGTs into broader neuromorphic networks, making them a viable option for wearable and portable electronics.[154] Devices like flexible dual-gate transistors incorporating natural materials have shown that these devices can be scaled to cover large areas while still supporting complex neuromorphic functions.[153]

The use of organic materials further contributes to EGTs' performance stability and scalability. Electrolytes based on nontoxic and biodegradable polymers, such as poly(vinyl alcohol) (PVA), offer excellent ionic conductivity and mechanical flexibility.[154] Devices using these organic electrolytes have demonstrated significant energy efficiency, capable of operating at extremely low power levels, as low as 1.16 fJ per operation.[154] This low energy consumption is a critical factor for neuromorphic systems, where large-scale operation must be balanced with the need for sustainability and reduced power use.

EGT large-area device processing, on the other hand, benefits from solution-processable materials, allowing for scalable fabrication techniques such as inkjet printing or spray deposition.[120,150,153,155,156] These methods enable the production of uniform devices without sacrificing performance. Additionally, advances in patterning and deposition techniques have enhanced the precision with which EGT components can be arranged over extensive surfaces, ensuring consistent electrical characteristics across the entire device.

## Synaptic functions

To reproduce learning and memory functions in an artificial brain, a presynaptic voltage spike must be applied to the device. In a 2-T configuration, the presynaptic spike is applied on one electrode (a presynapse) and read by the other electrode (a postsynapse). In a 3-T configuration, a presynaptic signal is applied to the gate electrode, and the postsynapse response is measured between the source and drain electrodes. When a short presynaptic voltage spike is applied, the current sharply increases (EPSC) and returns to its initial value (Fig. 5a). If two consecutive spikes are applied with a time interval $\Delta t$, the second postsynaptic current can exhibit a PPF (or PPD) response, Fig. 5b. This means the second voltage spike increases (PPF) or reduces (PPD) the current induced by the first spike. The intensity of facilitation or depression depends on $\Delta t$ and is usually defined as $100 \times \frac{A_2}{A_1}$, where $A_1$ and $A_2$ are peak intensities of the first and the second synaptic currents, respectively.[21,23]

Artificial synapses should mimic various behaviors observed in biological systems, such as the asymmetric Hebbian learning

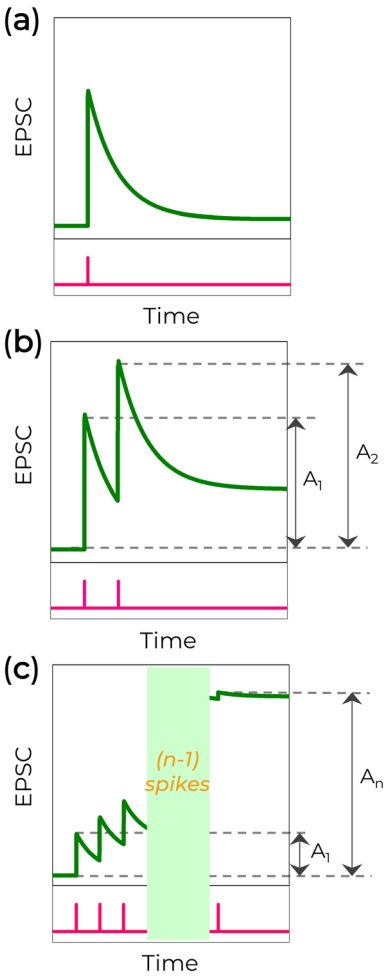


Fig. 5 Representation of a spike-dependent plasticity behavior for the emulation of synaptic responses. (a) Single excitatory postsynaptic current (EPSC). (b) Paired-pulse facilitation. (c) Long-term potentiation triggered by n spikes.

process (Fig. 2c, left). This learning rule is characterized by the relationship:[15,23,123]

$$\Delta w = \begin{cases} A_+ e^{-\frac{\Delta T}{\tau_+}} & \Delta t > 0,\ A_+ > 0 \\ B_- e^{\frac{\Delta T}{\tau_-}} & \Delta t < 0,\ B_- < 0 \end{cases}$$

where $A_+$ and $B_-$ denote the learning rates. $\Delta T$ represents the temporal difference between pre- and postsynaptic spikes ($\Delta T = t_{post} - t_{pre}$), which adjusts $w$. $\tau_+$ and $\tau_-$ define the time learning windows ($\Delta T$) during which potentiation and depression are significant. When the presynaptic spike precedes the postsynaptic spike ($\Delta T > 0$), the synaptic weight increases (potentiation, $\Delta w > 0$). Conversely, when the presynaptic spike follows the postsynaptic spike ($\Delta T < 0$), the synaptic weight decreases (depression, $\Delta w < 0$). However, in cases where $\Delta T < 0$, the asymmetric Hebbian learning rule may not be suitable, as it would undesirably strengthen the synapse. Instead, an asymmetric anti-Hebbian learning rule (Fig. 2c, middle left) would be more appropriate in such scenarios.[15]

Synaptic potentiation and depression through artificial synapses can also occur *via* SRDP, defined as the ratio $100 \times \frac{A_n}{A_1}$, where $A_1$ and $A_n$ represent the peak intensity of the first and the $n$th synaptic currents, respectively (Fig. 5c). This parameter depends on the spike rate[118,123] and the number of presynaptic spikes, which can shift from STP to LTP.

With an increase in presynaptic spikes within a specific timeframe, the parameter $w$ increases. When spikes cease, $w$ gradually decays and stabilizes at a frequency threshold, maintaining this state for an extended period (Fig. 5c).[21,23,118,123] In such conditions, fewer signal stimuli can reinforce the behavior, aligning retrieval and rehearsal steps in Fig. 2b. In addition to STDP and SRDP, spike-voltage-dependent plasticity and spike-duration-dependent plasticity have also been observed, showing similarities in learning rules between natural and artificial neural systems.[157]

In evaluating synaptic devices, their performances should be assessed based on STP, LTP, and spike-dependent plasticity. To replicate natural brain function effectively, artificial synapses must meet specific criteria: operating voltage below 1 V, power consumption less than 10 nW, and switching energy below 1 pJ per event.[54,158] Additionally, device size should not exceed 1 $\mu m^2$ for practical integration into compact arrays. Also, ideal operational parameters consider the write/read speeds faster than 1 μs, retention times exceeding 1000 ms, and durability through at least $10^3$ training cycles for memory enhancement.[54,158] Stability across varying temperatures is also crucial, influenced by the device's architecture and materials.[54]

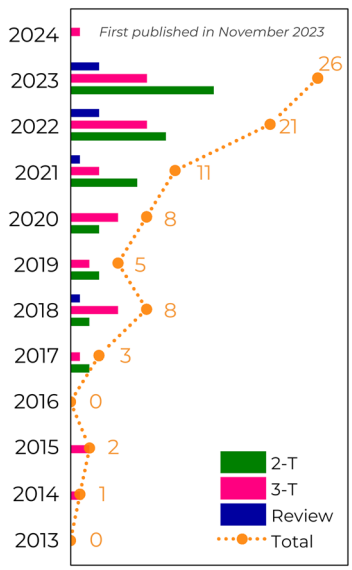


Fig. 6 Evolution of published research articles on biomaterial-based neuromorphic devices until December 2023. Our survey was achieved by using terms like "neuromorphic device", "artificial synapses", "memristive synapses", "synaptic transistor", "biomaterial", and "natural material" in Web of Knowledge, Scopus, and Google Scholar databases. Duplicated articles and articles without any evaluation of synaptic function (*i.e.*, reports evaluating only memory behavior) were removed from our analysis.

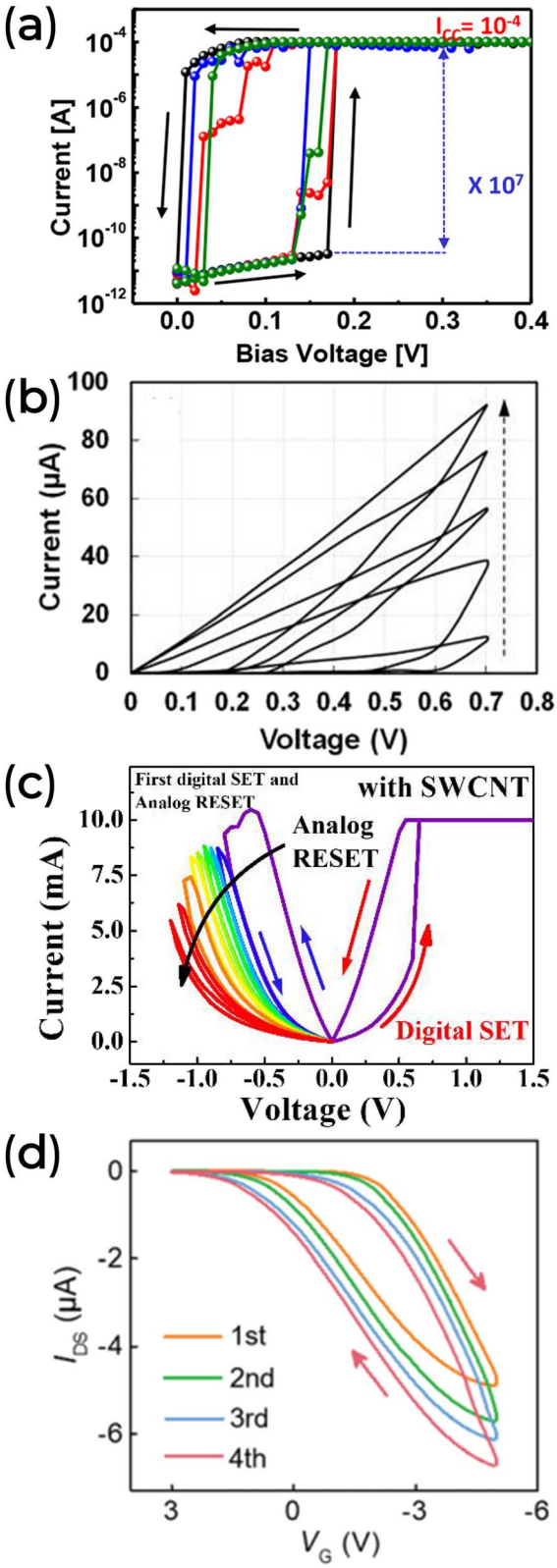


Fig. 7 (a) Threshold digital switching characteristic of a Pt/ι-carrageenan/Ag device. Reprinted with permission from M.-K. Kim and J.-S. Lee.[66] Copyright 2018, American Chemical Society. (b) Analog switching characteristic of an ITO/Honey/Ag device. Reprinted with permission from B. Sueoka *et al.*[78] Copyright 2022, AIP publishing. (c) A hybrid switch behavior on the Pt/$SiO_2$@SWCNT@Chitosan/Ti device. Reprinted under the Creative Commons Attribution (CC BY) license from J.-G. Min and W.-J. Cho.[73] (d) Transfer characteristics of a synaptic transistor using Dextran T500 as the dielectric layer. Reprinted with permission from Y. Yang *et al.*[133] Copyright 2020, Royal Society of Chemistry.

## Biomaterial-based neuromorphic devices

Natural biomaterials encompass a variety of materials found in nature, such as polysaccharides (like alginate, cellulose, chitosan, pectin, and starch), polypeptides (such as silk, collagen, and reflectin), small molecules (including β-carotene, chlorophyll, indigo, and nucleobases) and macromolecules (such as melanin, proteins, lipids, DNA, RNA, shellac and lignin). These biomaterials are characterized by their environmental sustainability and eco-friendliness, as well as their mechanical robustness, flexibility, optical transparency, lightweight, and semiconductivity or ionic conductivity. Their combination of properties makes them highly attractive for developing greener technologies.

In particular, these biomaterials show promise for integration into neuromorphic electronic devices, both as substrates and in dielectric and active layers (see Tables 1 and 2). Exploring their neuromorphic functionality is a relatively recent area of research, as evidenced by the scarcity of studies before 2014 (Fig. 6). However, there has been a notable increase in published articles over the past decade, indicating growing interest and investment in exploring these applications.

As previously mentioned, evaluating the device's memory properties is crucial. In a 2-T architecture, the memory behavior is observed through *I*–*V* curves, which can exhibit either gradual (analog) or abrupt (digital) resistive switching. In digital resistance switching (Fig. 7a), memory behavior resembles binary storage. Conversely, from an analog perspective, the gradual change shown in Fig. 7b indicates multilevel data storage similar to biological synapses.[159] Interestingly, a chitosan composite with $SiO_2$ and SWCNT demonstrates digital memory behavior during a set of processes and analog behavior during the reset process (Fig. 7c).[73] This behavior was ascribed to the electrochemical reaction between the chitosan electrolyte and mobile ions, with the SWCNT aiding the formation of a metallic conductive filament (ECM). In a 3-T architecture, the electrical response of a synaptic transistor is analyzed through its transfer characteristics. The goal is to observe the response of the postsynaptic current ($I_{DS}$) to a presynaptic excitation ($V_{GS}$). Analogous to memristors, memory behavior in this context is analyzed by examining the variation in $I_{DS}$ with the changes in $V_{GS}$ (Fig. 7d).

Once the resistive switching properties are obtained, the synaptic properties (plasticity, pair-pulse facilitation, and spike-dependent plasticity) can be verified. Unlike the electrical response, 2-T and 3-T devices yield similar synaptic behavior.

One important neural information is the combination of all the inputs the synaptic device receives. This is known as synaptic integration[160] and allows the integration of excitatory and inhibitory signals at any moment to determine whether an

action potential is generated. The traditional approach is the temporal summation between neurons. Pulses of different amplitudes and time intervals can emulate short-term synaptic plasticity and PPF or PPD. For example, we present the work of W. Qin *et al.*, which studied maltose-ascorbic acid electrolyte-gated synaptic transistors (MAEGST).[136]

Fig. 8a depicts the EPSC response of MAEGST under varying gate voltage amplitudes (0.3, 1, 2, and 3 V) applied to the electrolyte for 10 ms intervals at $V_{DS}$ of 0.1 V. When a positive bias (0.3 V) stimulates the system, ion migration and EDL formation increase the channel conductance by ~4 μA. Upon removal of the stimulus, conductance slowly returns to its initial value of about 31 μA. Increasing the pulse amplitude ($V_G$) to 5 V raises the EPSC to ~56 μA (Fig. 8b), with the amplitude not decaying to the initial value after that. Pulse duration similarly affects EPSC response.

The pulse duration also changes the EPSC response. While maintaining $V_G$ at 1 V, the authors varied pulse duration from 10 to 60 ms. Fig. 8c and d demonstrate that as pulse duration increases, the rise in EPSC amplitude slows down. This behavior reflects the modulation of the channel's conductance and the EDL formation, where ion motion at the MAE/ITO-electrode interface saturates. These dynamics resemble those observed in biological synapses, suggesting a transition from STP to LTP.

Biomaterial-based neuromorphic devices can demonstrate SNDP to replicate learning and forgetting processes. In Fig. 8e, the EPSC increased with the number of spikes applied to the

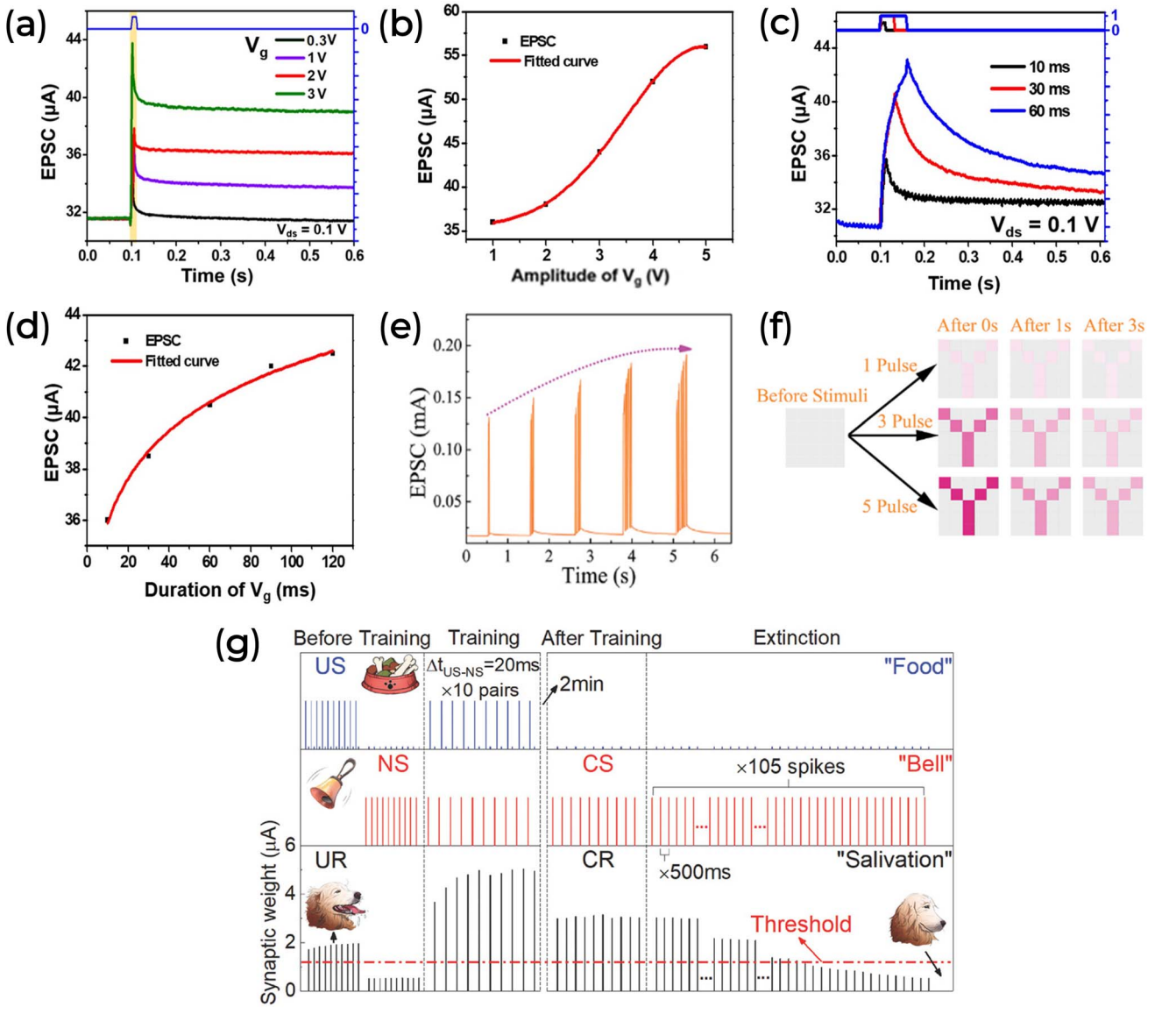


Fig. 8 (a and b) EPSC using different gate voltage pulse amplitudes and same time interval (10 ms). (c and d) EPSC using 1 V of gate voltage pulse amplitude and different time intervals. (a–d) Adapted with permission from W. Qin *et al.*[136] Copyright 2021, American Chemical Society. (e) EPSC under different spike numbers. (f) The learning-and-forgetting patterns of an ITO/Albumen@CuO/Ag synaptic device by SNDP. (e and f) Reprinted with permission from T. Guo *et al.*[61] Copyright 2022, John Wiley and Sons. (g) Based on Pavlov's dog experiment, change in synaptic weight resulted from the associative learning process. Reprinted with permission from F. Yu *et al.*[123] Copyright 2018, John Wiley and Sons.

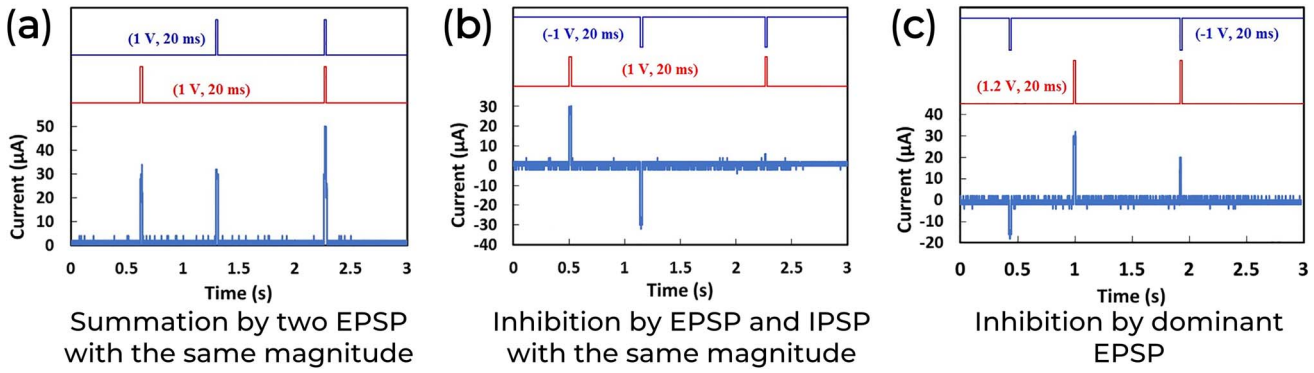


Fig. 9 Synaptic integration in a spatial summation configuration of an ITO/Honey/Ag 2-T neuromorphic device. Adapted with permission from B. Sueoka *et al.*[78] Copyright 2022, AIP publishing.

ITO/Albumen@CuO/Ag device.[61] This behavior is illustrated in Fig. 8f, where 25 of these devices, arranged in a 5 × 5 pixel array, could encode a "Y" image.[61] As more spikes were used to stimulate the array, the image's contrast, represented by the darkening of the pink color, increased, mimicking the learning process. Subsequently, the pink color faded after stimulation, demonstrating the forgetting process. Higher spike counts maintained the image contrast longer, suggesting, once more, a transition from STP to LTP.

The learning process of a biomaterial-based neuromorphic device was also evaluated by classical conditioning in physiology by F. Yu *et al.*[123] This associative learning process involves pairing a conditioned stimulus (CS) with a neutral stimulus (NS) and/or unconditioned stimulus (US) through repeated pairings. To clarify this association, F. Yu compared his study to Pavlov's dog experiment, where an initial bell ring (NS) does not cause any response, such as salivation, in the dog, whereas food (US) does. By ringing the bell before feeding the dog, an association formed between NS and US (now CS) triggers salivation. However, the CS effect diminishes if the US is not presented over the timer (Fig. 2b). In an artificial environment, such as the chitosan-based synaptic transistor proposed by Yu, the synaptic weight can be adjusted by controlling the timing between two pulses. Here, the applied pulse voltage ($V_G$) represents the "bell ringing," and the $V_{DS}$ the "sight of food." When a $V_{DS}$ pulse is applied, the output response ($w$) increases above the threshold (Fig. 8g), analogous to "salivation" in the dog experiment. Without constant US stimulation, the amplitude $w$ can diminish over time.[123]

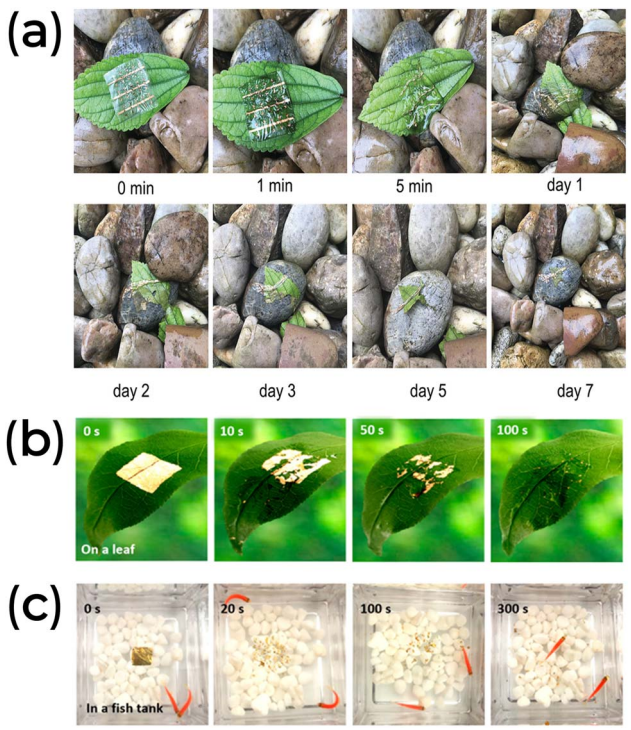


Fig. 10 (a) The degradation process of a chlorophyll-a/SWCNT composite transistor in a natural environment. Reprinted with permission from Q. Ou *et al.*[130] Copyright 2021, John Wiley and Sons. (b and c) The pectin-based synaptic transistor degradability. Reprinted with permission from Y. Li *et al.*[139] Copyright 2022, American Chemical Society.

Another way to achieve synaptic integration is through spatial summation. The spatial summation involves the addition of presynaptic positive or negative input voltage spikes, which simulate excitatory or inhibitory postsynaptic potential (EPSP or IPSP). The basic idea is that when two presynaptic EPSPs coincide, the postsynaptic response should combine these initial stimuli (Fig. 9a). It is important to note that, similar to biological systems, where some energy is used to generate an action potential, the current measured by the device is lower than the mathematical sum of the inputs. IPSP also plays a role in signal processing by suppressing unwanted signals and limiting the flow of information (Fig. 9b). When EPSP and IPSP co-occur, the result is dominated by the one with the highest magnitude, or the postsynaptic remains silent (Fig. 9c). B. Sueoka *et al.* demonstrate that a Honey-based neuromorphic device could exhibit a spatial summation (Fig. 9).[78]

When considering a healthcare device, it's crucial to analyze other characteristics. Unlike some synthetic biodegradable materials that only partially disintegrate, biomaterials have been part of the ecosystem for millions of years. Such a long presence has allowed bacteria and fungi to develop enzymes that efficiently degrade them.[26,161–163] For instance, cellulose, a common natural material used in soft electronics, can be

degraded by cellulases, which are cellulolytic enzymes.[161] The complete fragmentation of these materials into water, carbon dioxide, and other organic molecules makes them ideal for transient electronics. These devices can alleviate environmental concerns and are safe for *in vivo* applications.[163–165]

Transient electronics are systems designed to dissolve after serving their purpose or when triggered by specific physical or chemical conditions.[4,6,26,163,165–167] This feature is crucial for advancing wearable sensors' sustainable and low-cost mass production. In a biomedical setting, these devices offer a significant advantage over traditional ones. They can be absorbed within the body, avoiding traumatic and invasive removal surgery and reducing (bio)e-waste.[4,26,165,167]

Biomaterial-based neuromorphic devices have demonstrated potential for degradability.[81,91,130,132,135,139,148] Fig. 10a illustrates a neuromorphic device that uses a chlorophyll/SWCNT transistor configuration on a PVA substrate. This device is placed on a green leaf and left in a rainy outdoor environment to simulate the effect of natural degradation. The PVA matrix swelled within the first five minutes, significantly deforming the Au electrodes.[130] The decomposition of the system was observed over a week and compared to the natural leaf. Photographs from days 1 to 7 show the apparatus deteriorating, confirming its degradability in a natural environment. The authors noted that the metallic Au electrodes and the SWCNT layer did not dissolve in the rainwater and would not harm the environment.[130] However, they also point out that Au is a finite and critical material for electronics.

Similarly, a transistor made from apple pectin completely decomposed within 100 s when exposed to dripping water, Fig. 10b.[139] When immersed in a fish tank, the same system degraded in less than 20 s due to the water tension, and its components either sank to the bottom or were eaten by the fish, Fig. 10c.[139] The lifetime of biomaterial synaptic devices typically ranges from a few minutes to a couple of hours, which can limit its applications. To extend their lifespan, coating layers are used to prevent the materials from coming into contact with dissolving agents. Additionally, degradable substrates like silk, whose transient properties can be adjusted through chemical treatment or thermal annealing, can last several months. These coating layers are usually made from synthetic elastomers, though some examples based on biomaterials do exist.[168,169]

The last transient example highlights another critical property for healthcare applications: biocompatibility. Biocompatibility refers to a material's ability to perform its intended function without causing reactive inflammatory responses on the host biological system, both in short-term (transient) and long-term interactions.[20,26] In the fish tank experiment, animals maintained stable vital signs even after a week under the same experimental conditions, demonstrating the system's non-toxicity.[139] To further evaluate the toxicity, the authors tested the pectin solution in cell culture solutions for two days (Fig. 11a). Fluorescent images of the stained cells showed normal proliferation and high viability (low concentration of dead cells, shown in red). In another example, the cytotoxicity of neuromorphic devices based on hyaluronic acid (HA) was compared to a similar device based on PEDOT : PSS. The HA-based neuromorphic device showed no cell cytotoxic reaction, unlike the PEDOT : PSS (Fig. 11b).[81] Fluorescence-activated cell sorting was used to quantitatively assess cell viability between the devices, revealing an average damaged cell ratio of about 5.7% for the HA-based neuromorphic device, compared to 41.3% for the PEDOT : PSS device.[81] This demonstrates the superior biocompatibility of natural materials over standard synthetic materials.

Similar to what has been demonstrated for other devices, the mechanical properties of a neuromorphic device intended for implantable and wearable applications are crucial for matching the strength and elasticity of the body's native soft tissues.[170,171] Flexible, bendable, and stretchable substrates are usually mandatory for these applications. Bio-based semiconductors are also being considered for their suitable mechanical features. Natural materials such as cellulose[118,119,126] and silk fibroin[93,172] are integrated into flexible (Fig. 12a and b) and conformable (Fig. 12c) substrates for neuromorphic applications. Chitosan[127] and sodium alginate[145] are also used as substrates in these settings. These materials offer softness, biocompatibility, and biodegradability, advancing sustainable development in intelligent healthcare applications. Additionally, Zein, extracted from maize, has been used in the active layer of a flexible 2-T device by Y. Kim and co-workers, demonstrating excellent mechanical stability.[101] Their device maintained recognition accuracy even under bending mechanical stress (Fig. 12d).

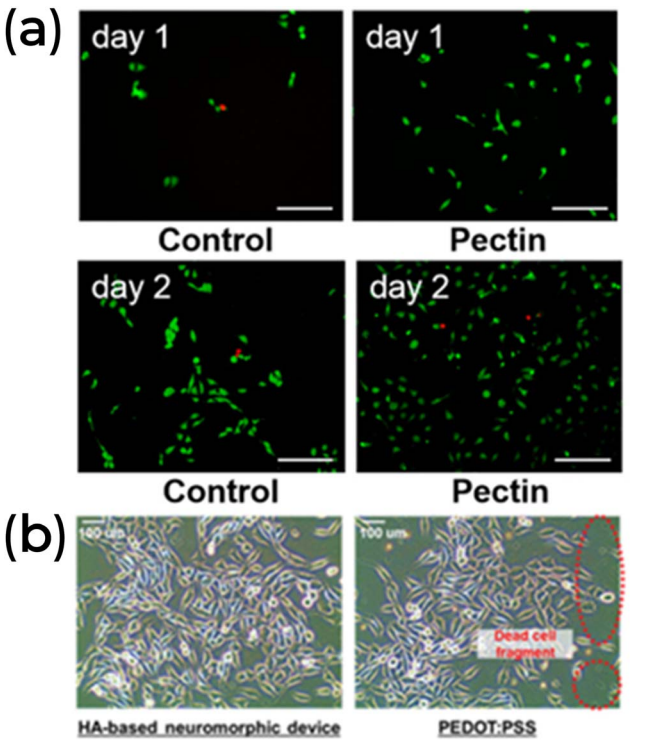


Fig. 11 (a) The pectin-based synaptic transistor biocompatibility. Reprinted with permission from Y. Li *et al.*[139] Copyright 2022, American Chemical Society. (b) Optical images of a cytotoxicity test of HA-based and PEDOT : PSS neuromorphic devices. The highlighted area in the right panel shows the dead cell fragments. Adapted with permission from J. H. Lee *et al.*[81] Copyright 2021, John Wiley and Sons.

In a direct example of biomimetic application, biomaterials have been used as artificial organs capable of sensing light signals as input. Light has been shown to enhance the STDP and SRDP functions of artificial photonic synapses (Fig. 13a and b), and it can be used for image recognition (Tables 1 and 2). C. Zhang *et al.* advanced this concept further by constructing a concave hemispherical artificial retina using orange peel pectin as a dielectric layer in a 3-T device (Fig. 13c).[140] Their 3D artificial retina can mimic the human visual system's image sensing and preprocessing function. It was designed with a concave hemispherical device array to project an arrow image in the four cardinal directions (north, south, west, and east), as shown in Fig. 13d. The arrows were accurately mapped without aberrations and vignetting, simulating a proper response of the human eye.

## Opportunities in healthcare

As mentioned in Section 2.1, the PNS in biological systems recognize and respond to chemical, light, pressure, and sound stimuli, transmitting this information to the CNS and the rest of the body. Similarly, a neuromorphic electronic system that mimics these functions could be used in various applications, including brain-computer interfaces, biosensing, health monitoring, bioinformatics, computing, exoskeletons, neuroprosthetics, sensorimotor neural signal transmission, and soft robotics. Developing artificial CNSs and PNSs requires creating neuromorphic devices that can be integrated into interconnected systems, detecting external stimuli and responding to environmental changes.

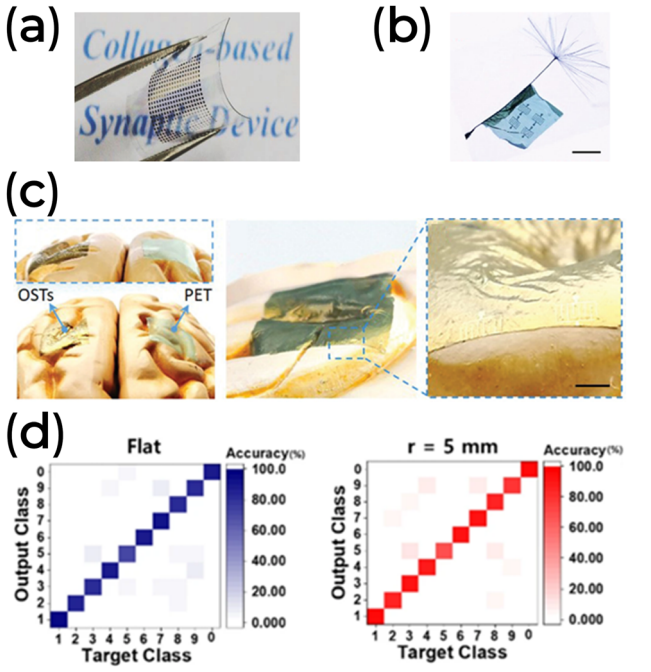


Fig. 12 (a) The flexible collagen-based 2-T synaptic device. Reprinted with permission from N. Raeis-Hosseini *et al.*[75] Copyright 2018, John Wiley and Sons. (b and c) The 3-T synaptic device is based on biomaterials wrapped around a dandelion seed and is conformable to a human brain model. Adapted with permission from Y. Yang *et al.*[132] Copyright 2020, John Wiley and Sons. (d) Inference and learning feature of the ITO/Zein/Al synaptic device under different bending conditions. Reprinted under Creative Commons Attribution 4.0 International License from Y. Kim *et al.*[101]

Implementing such devices in healthcare requires excellent mechanical compliance, including softness, conformability, flexibility, and stretchability, as they are integrated directly into biological bodies, human skin, or fabrics and must ensure proper signal transmission.[8,173–177] For instance, a knee can stretch up to 55% of its initial size during motion, meaning that a nearby device must support both bending and stretching forces and allow joint activity.[174,178–180] In this context, the biocompatibility and mechanical flexibility of biomaterials make them suitable for matching the biological environments and tissues while maintaining low-power efficient computing.

Biomaterial composites have demonstrated their ability to accurately and in real-time detect human electroencephalogram (EEG),[181–184] electrocardiograph (ECG),[185–189] and electromyography (EMG) signals.[190–193] For example, an FDA-approved naturally derived type-A gelatin (acid-treated collagen) has been used as a paintable biogel for on-skin EEG detection due to its water-solubility, biodegradability, good biocompatibility, and large-scale production. To enhance its performance, this biogel was combined with biocompatible functional components such as sodium chloride, sodium citrate, and a water-glycerol binary solvent system, improving its ionic conductivity, ionic cross-linking, and long-term stability.[183] This composite exhibited a thermo-dependent phase transition from viscous fluid to viscoelastic gel (Fig. 14a), adhered well to the skin (Fig. 14b), and provided a reliable interface with a hairy scalp (Fig. 14c). In its solid-like gel form, the biogel could detect EEG alpha activity from the occipital region of a hairy head, with no significant difference in signal shape, signal amplitude, and power spectral density compared to commercially available EEG paste (Fig. 14d).[183]

Similarly, an electronic tattoo (e-tattoo) made from graphene, $Ca^{2+}$ ions, and silk fibroin demonstrated self-healing and multi-stimulus sensing capabilities.[186] This e-tattoo could detect changes in temperature and humidity while providing a high signal-to-noise ratio for monitoring the heart's rhythm and electrical activity (ECG signal). The quality of the ECG signal remained consistent before and after the self-healing process, indicating minimal disruption.[186] Additionally, a composite material comprising a porous cellulose derivative from grass and two-dimensional titanium carbide ($Ti_3C_2T_x$) MXene could record muscle electrical activity (EMG signal), simultaneously performing electrostimulation and electrothermal therapy.[191] This all-in-one muscle theranostic platform exhibited good air permeability and sweat stability, ensuring comfort for the patient.

Although the examples mentioned are not neuromorphic platforms and are only partially sustainable due to their additives, they prove that natural biomaterials can integrate into advanced healthcare systems. There is still significant room for exploring innovative device and circuit concepts and identifying new material options.

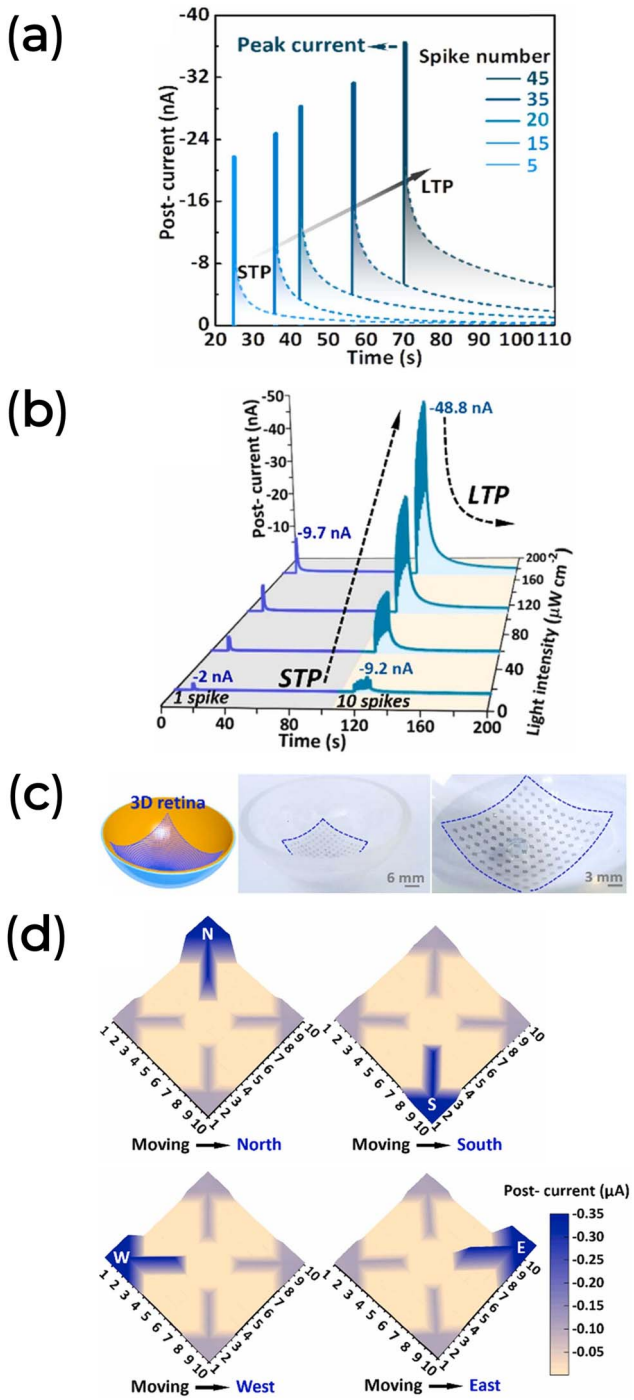


Fig. 13 (a) EPSC response to spike number under fixed light width, frequency, and intensity (1 s, 5 Hz, and 56 μW $cm^{-2}$, respectively). (b) EPSC response as a function of the light intensity of a sequence of one single spike (1 s light width) followed by ten spikes (1 s light width at 5 Hz frequency). (c) Concave spherical artificial retina based on orange peel pectin conformable synaptic transistor array. (d) Response of the 3D artificial retina recognizing the four cardinal directions. Data adapted with permission from C. Zhang *et al.*[140] Copyright 2022, Elsevier.

Bioelectronic circuits[194] are rapidly advancing alongside the sensing capabilities of OECTs, making them ideal for developing intelligent processing in on-body devices. These devices can interact with users to effectively predict and communicate general or specific information. However, in real-time healthcare applications, integrating biosensors, controlled drug delivery, and tissue repair present a significant challenge for biomaterials. This challenge arises from the need to interface complex biological systems – dominated by membrane electric potential gradients, local chemical reactions, and ionic gradients and currents – with traditional semiconductor devices that typically operate in a manner that may be detrimental to natural tissues.[8,11,31] Therefore, developing systems capable of accurately translating ion signals into electronic signals (known as iontronics) becomes crucial. One promising approach involves OECTs, facilitating seamless integration between biological systems and electronic devices. Alternatively, designing suitable biomaterials could also address these challenges. However, achieving effective electronic coupling between ions and electrons remains a significant hurdle, which is not a common property of natural or synthetic materials.[195]

In bioelectronics, biological processes transmit signals to electronic devices, which can, in turn, initiate physiological responses through chemical or electrical stimuli. Traditional healthcare systems often rely on enzymatic reactions to modulate the current flow in biosensors. The measured level can be managed by an external agent (Fig. 15a) or in a closed-loop manner (Fig. 15b). These biosensors measure parameters like glucose levels in diabetes management. For instance, in one approach, a small blood sample reacts with the biosensor to measure glucose, informing the patient to take medication as needed. In contrast, a closed-loop system continuously monitors glucose levels, automatically administering medication when required. However, these approaches overlook dynamic factors such as exercise and diet, which influence glucose levels over time. Future healthcare systems must be adaptable and responsive to multiple variables to address this, potentially leveraging neuromorphic systems for enhanced performance (Fig. 15c).[196]

Combining bioelectronic and neuromorphic platforms has significant potential for autonomous healthcare applications. In implantable devices, neuromorphic systems with adaptable input variables could locally measure and process biologically. This allows the platform to learn and respond to analyzed behaviors in real-time. In contrast to traditional methods that process biological signals remotely, which can risk losing critical information without high bandwidth, this approach integrates artificial synapses and closed-loop systems.[196] These innovations are promising for long-term applications such as restoring sensory functions and treating neurodegenerative diseases like Alzheimer's and Parkinson's. Such a technology could enhance communication between organs and regulate physiological processes by replacing biological neurons with artificial neuronal cultures on multi-electrode arrays. Moreover, it may stimulate cell regeneration in damaged tissues.[197–199]

Additional bioelectronic application prospects could also rely on human–machine interactions (HMI), with human electrophysiological or motion signals leading to the realization of robot control, personal device control, and even virtual reality. Silk protein-based electronics[200,201] and hydrogel[189] are

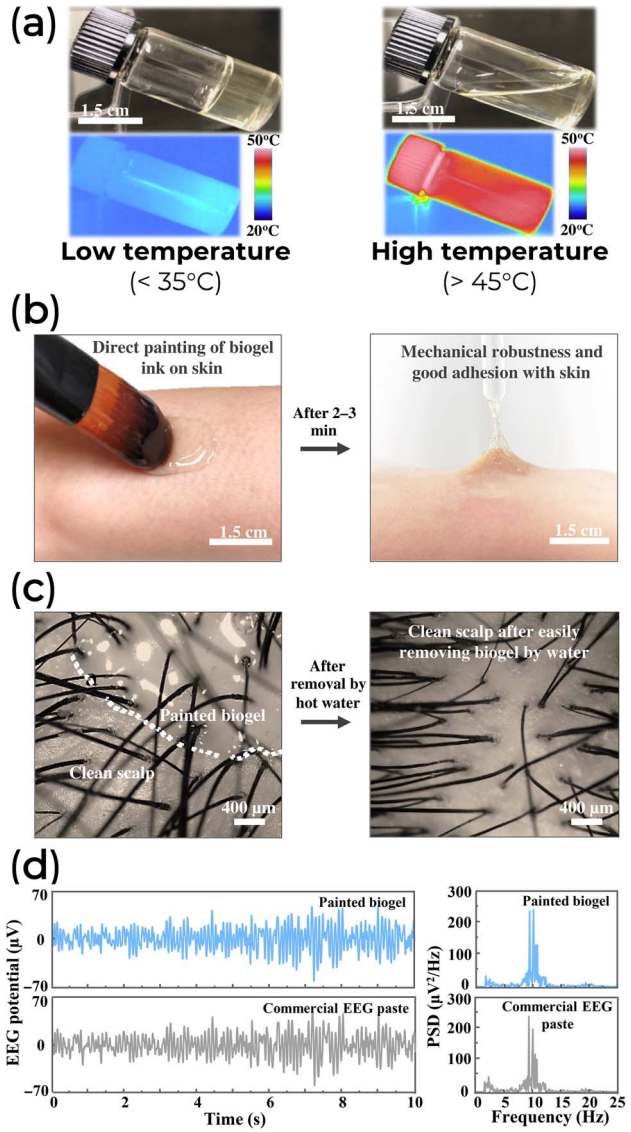


Fig. 14 (a) The transition of the biogel between fluidic and solid-like states at different temperatures. (b) On-skin painting and adhesion capability of the biogel ink. (c) A good contact of biogel painted with hairy scalp and its easy removal by hot water. (d) EEG alpha rhythms (left) and power spectral density analysis (PSD, right) comparison between the painted biogel (top) and a commercial past (bottom). Adapted from Creative Commons Attribution 4.0 International License from Chunya Wang *et al.*[183]

promising progress toward these HMI applications. For instance, a silk-based system can collect an input signal from human fingers processed by an artificial neural network and transfer the output signal to a robotic hand (Fig. 16a). One thousand twenty-four total gestures were obtained based on different degrees of bending from the fingers of both human and robot joints (Fig. 16b).[200]

Similarly, a silk-based wearable five-finger nanogenerator showed promise in converting finger tapping into electrical signals coded into 26 English letters. Jiarong Liu and collaborators explored a direct healthcare application: overcoming the communication barrier between doctors and patients who cannot speak. In this sense, the patient used the keyboardless system to express their thoughts precisely by moving the fingers following the code within the finger input interface.[201]

In electroceuticals, wearable and implantable electrodes (WIE) show great potential to enhance the lifespan and improve quality of life, as they can decode the electrophysiology of cells and tissues, opening up a range of therapeutic applications. For example, a typical WIE can effectively address muscle spasms, alleviate pain, improve rehabilitation after spinal cord injuries, and promote the healing of chronic wounds through targeted electrostimulation.[202–205] Hence, combining WIE with neuromorphic systems makes the next generation of intelligent and modern healthcare platforms flexible, discreet, comfortable, portable, and remote. This could allow a connection between precise *in vivo* monitoring of health conditions inside the body, connection gadgets, and therapeutic response (closed-loop system).

The WIE's wide application in sensing and therapeutic applications relies on power sources for continuous operation.[206] Ensuring long-term biocompatibility and biosafety is crucial for their implementation in clinical applications.[202,204] Here, biomaterials also garner attention. In addition to the environmentally friendly and economic features, biomaterials also have inherent characteristics of shaping customization, large surface area, and many active sites — essential attributes for stable capacitance retention with a potential increase in the electrode's specific capacitance.[207,208]

## Opportunities in bio-based and hybrid materials

The advanced technology mentioned above requires the development of electro-active materials with multifunctional properties, such as being lightweight, having good mechanical properties (flexibility and stretchability), and being a good material for powering devices.

Among numerous candidates, one natural biomaterial stands out: melanin. Melanin is a pigment that occurs naturally across various life forms, ranging from viruses and fungi to plants and mammals. In humans, melanin (especially its subgroup eumelanin) is notably present in the hair, skin, inner ear, eye, and brain.[31,209] It plays critical roles, such as providing pigmentation, acting as an antioxidant, and offering protection against noise, UV light, and abrasion.[31,210] From a technological perspective, melanin has hydration-dependent conductivity[211–214] that can sustain protonic current,[215–217] processability into flexible substrates,[218,219] and transduce ionic signals into electronic ones.[219–221] Additionally, melanin demonstrated memory-like behavior,[222,223] the propensity to form electrochemical metallization bridges between metallic electrodes,[224,225] and photoconversion[226] and energy storage capabilities.[218,227–229] In regards to powering electronics, the melanin anode, in combination with the manganese oxide cathode, was able to supply 5 mW of power for up to 20 h, while the melanin cathode with a sodium–titanium phosphate anode

provided 18 mW for 16 h, which adequately fulfilled the power needs of a variety of existing medical devices.[230]

Melanin's inherent biocompatibility[231,232] and biodegradability,[233,234] combined with the development of flexible,[218,219,235,236] stretchable,[237,238] and self-healing[237,239] devices, represents a promising frontier in bioelectronics and sustainable healthcare technologies, particularly in wearable and implantable applications. Notably, it has been demonstrated that melanin can form dynamic networks capable of restoring mechanical integrity after damage.[239] This self-healing ability is vital for the longevity and reliability of flexible devices, especially in scenarios where mechanical stress and strain are frequent.

Collectively, all these features make melanin attractive for neuromorphic and sustainable healthcare systems. Nonetheless, the potential use of melanin in medical settings is in the early stages,[209,219,235,239–242] with no study yet exploring its synaptic potential.

Although natural melanin is beginning to appear in the literature, many proof-of-concept applications still rely on synthetic melanin derivatives. This trend persists because synthetic derivatives can be engineered to have properties similar to natural materials but without the biological impurities that can hinder device efficiency.[209] Synthetic melanin eliminates these impurities and ensures more consistent and reliable device performance.[243] Additionally, the ability to tailor its properties through chemical modifications and processing techniques is crucial for achieving any desired functionality.[31,209,244,245] Tailoring involves manipulating the molecular structure or incorporating specific functional groups or exogenous parts to enhance the material's performance, such as increasing its electrical conductivity, mechanical strength, or biocompatibility. This adaptability is critical to meeting the diverse requirements of different health applications, from wearable devices to implantable systems.

While natural materials like melanin offer exciting possibilities, it is essential to acknowledge that not all natural or biodegradable materials are sustainable, as sustainability extends beyond biodegradability and encompasses the environmental impact throughout a material's lifecycle – from extraction and processing to end-of-life disposal.[209] For example, cellulose, a natural polymer derived from renewable sources like wood pulp, is celebrated for its biodegradability and eco-friendly characteristics.[165,246,247] In contrast, although natural latex does not degrade seamlessly, its processing and disposal can still have environmental repercussions.[247] This highlights the importance of distinguishing between natural and genuinely 'green' materials.

Natural materials are derived directly from biological sources, whereas green materials originate from renewable sources and ensure minimal environmental harm during their entire lifecycle. This distinction is crucial for advancing sustainable technologies.

The quest for sustainable materials goes beyond biodegradability; it also involves ongoing innovation to find alternatives that offer high performance without compromising the environment. Scientists and engineers are continually exploring

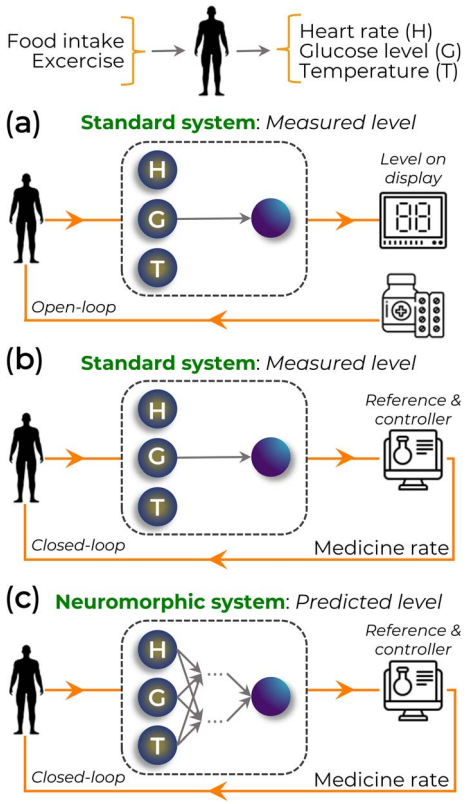


Fig. 15 Schematic of (a) open-loop and (b and c) closed-loop systems based on bioelectronics sensing, inspired by.[196] These systems (a and b) are related to the traditional method of measuring the glucose level without considering other parameters. In (c), the glucose level is estimated considering multiple and interconnected variables.

new ways to combine desirable properties in efficient and eco-friendly materials. This includes leveraging advanced technologies to modify natural materials and synthesize new compounds that overcome the challenges faced by traditional materials.[246–248] Combining specific physical and chemical properties can lead to significant advancements in various technological applications.

Hybrid materials, which combine organic and inorganic components, are emerging as innovative solutions that can be customized for diverse applications. These materials are designed to unite the best of both worlds: the flexibility and functionality of organic components with the robustness and stability of inorganics. This enables the creation of complex structures with adjustable properties, meeting any specific needs. The tailorability of these hybrid materials opens new frontiers in materials science, allowing the development of more efficient and sustainable solutions.

In this context, advanced porous coordination polymers such as metal–organic frameworks (MOFs) stand out as hybrid materials combining metal ions with organic ligands to form highly porous and customizable structures.[249–252] Due to their superior design flexibility and the ability to be customized, MOFs can be combined with various organic or inorganic materials to meet specific functions and performance criteria, which represents a significant innovation in the development of

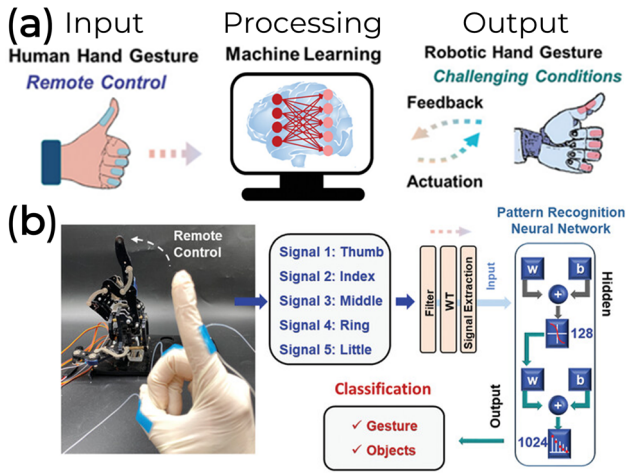


Fig. 16 (a) Schematic representation and (b) experimental apparatus of an intelligent human–machine interaction assisted by machine learning. These systems require a human hand gesture (input) to be processed and analyzed by an artificial neural network (processing) for gesture/object recognition and remote control of a robotic hand (output). Adapted under Creative Commons Attribution License from Mengwei Liu *et al.*[200]

new advanced materials systems and offers vast possibilities for the applications in environmental,[248] biomedical[253–255] and electronics[256–259] fields.

Building on MOFs' inherent versatility, these materials have emerged as promising candidates for developing neuromorphic devices.[259–261] Their ability to facilitate ionic and electronic conductivity and their customizable pore structures make them ideal for mimicking the complex signal-processing functions of biological synapses.

Recently, a humidity-mediated MOF-based memristor was built using an origami-like rolled-up metallic nanomembrane electrode.[260] The MOF-based rolled-up memristor exhibits stable ambipolar resistive switching with low power requirements. This performance is attributed to structural defects induced by water molecules, which introduce additional states within the bandgap region.

However, the practical use of MOFs is challenging. A primary challenge is achieving controllable resistance adjustments, necessitating that MOFs possess inherent conductivity and efficient electronic transport properties.[259] Moreover, they must demonstrate robust stability and adaptability for programmable and non-volatile memory storage.[259] To overcome these issues, MOFs' tailorability comes into play. By precisely engineering the composition and architecture of MOFs, it is possible to modify their molecular structure and functional groups to optimize their electronic transport properties and pore configurations, thereby fine-tuning their material characteristics and creating devices with improved performance to emulate the dynamic and adaptive nature of neural networks.

As the field advances, there is a significant push toward sustainability in MOF synthesis. Traditionally, MOFs are constructed from metal ions and organic components derived from non-renewable petrochemical sources, which pose toxicity risks and are unsuitable for healthcare applications.[262–264] This has led to the exploration of greener alternatives. Sustainable synthesis methods now emphasize using ligands from biomass, metals sourced through environmentally responsible practices, and ecological solvents like water and ethanol.[263,264] By integrating these sustainable practices, MOFs can be produced in a more environmentally friendly manner, minimizing their ecological footprint.

A notable advancement in this field is the development of Biological Metal–Organic Frameworks (Bio-MOFs).[252,265,266] These novel materials incorporate biomolecules such as amino acids, peptides, nucleobases, and saccharides derived from renewable and non-toxic sources. This innovation improves the biocompatibility of MOFs and utilizes biodegradable, renewable raw materials. Biologically derived ligands offer multiple coordination sites and functional groups that facilitate effective binding with metal ions, resulting in flexible and functional structures.[251] The inherent properties of these bio-ligands, such as easy availability, simplicity of synthesis, and inherent chirality, make them highly advantageous for diverse applications.

Polysaccharide-based bio-MOFs, for example, have gained significant attention for their biocompatibility and structural robustness, offering mechanical strength and flexibility.[267–269] The interaction between metal ions and polysaccharides enhances crystallinity, improving overall performance and demonstrating potential for creating functional composites suitable for various applications.

Recent studies have demonstrated the versatility of MOFs in biological contexts. For instance, a MOF based on yttrium (Y) and benzene tricarboxylic acid (BTYC), $Y(BTC)(H_2O)_6$, has been utilized to isolate hemoglobin from human blood.[270] This application opens new avenues for protein separation and medical diagnostics. Similarly, bio-MOFs derived from amino acids like L-serine have been employed in solid-phase extraction to detect and extract B vitamins.[271]

In biosensing, Pb-β-cyclodextrin-based bio-MOFs have emerged as promising candidates due to their water solubility and biocompatibility. These materials have been used to develop electrochemiluminescence immunosensors for insulin detection, highlighting their potential in medical diagnostics and monitoring.[272] Bio-MOFs' ability to integrate with biological systems further underscores their significance in advancing healthcare applications.

Despite these advancements, MOFs still face challenges related to stability. Traditional MOFs can hydrolyze in water or acidic/alkaline environments, releasing toxic ligands into the environment.[266] In addition to bio-MOFs, researchers have explored using biomass as a sustainable alternative to traditional carbon nanomaterials.[273,274] Being abundant, renewable, and cost-effective, biomass provides a stable link with MOFs through its rich hydroxyl and carboxyl content. This approach enhances MOFs' stability and offers a low-cost and sustainable strategy for preparing advanced functional materials. The rich heteroatom content in bio-MOF and biomass-based MOF derivatives enhances their electrochemical performance, making them suitable for neuromorphic applications.[251,256,257,259,265,275]

## Opportunities in device architecture

As mentioned before, OECTs are profoundly significant in bioelectronic and biomedical systems due to their ability to achieve high signal amplification and effective biomolecule detection. By optimizing the gate dielectrics, the performance and efficiency of organic field-effect transistors can also be significantly enhanced, further broadening the applications of these flexible devices. For instance, recent research has highlighted that the intrinsic gain of flexible OECTs can be notably affected by the device's size reduction.[276] This research used strain-engineered, extremely thin, self-supporting, and highly flexible nanomembranes as flexible substrates to construct flexible liquid-gated OFETs. These nanomembranes can be rolled into microcylindrical shapes, allowing the transistor to be fully incorporated within a hollow microtube (r-OECT), Fig. 17a. This innovative setup achieved exceptionally high intrinsic gain ($>10^4$) with superior signal output and amplification when compared to a planar configuration (p-OECT, Fig. 17b, transistor placed on a glass substrate). Such a response was ascribed to the dielectric confinement, enhanced electric field, and ion diffusion within the self-rolled device.[276]

In addition to improved performance, the r-OECT configuration was employed as a dopamine biosensor, a biomarker associated with neurological disorders.[276] During cyclic voltammetry testing in the dopamine solution, these devices exhibited significant sensitivity levels (~3 μM), aligning well with clinical concentrations expected in urine samples. This demonstrates the potential of strain-engineered nanomembranes as flexible substrates for developing healthcare devices.

Advanced rolled-up nanomembrane technology also enables the creation of susceptible pressure sensors. These devices feature an innovative architecture that allows for the precise adjustment of contact geometry and current injection at the nanoscale level.[277] This flexibility ensures the devices can effectively respond to mechanical forces applied to the top electrode (Fig. 17c), increasing the nanomembrane's active area without compromising the underlying semiconductor layer. Consequently, variable-area transport junctions (VATJs) exhibit remarkable sensitivity to high-pressure detection, achieving up to 480 $kPa^{-1}$ and rapid sensor response times.[277] Recent advancements in synaptic transistors, with a sensitivity of 80 $kPa^{-1}$, have shown significant potential in transforming

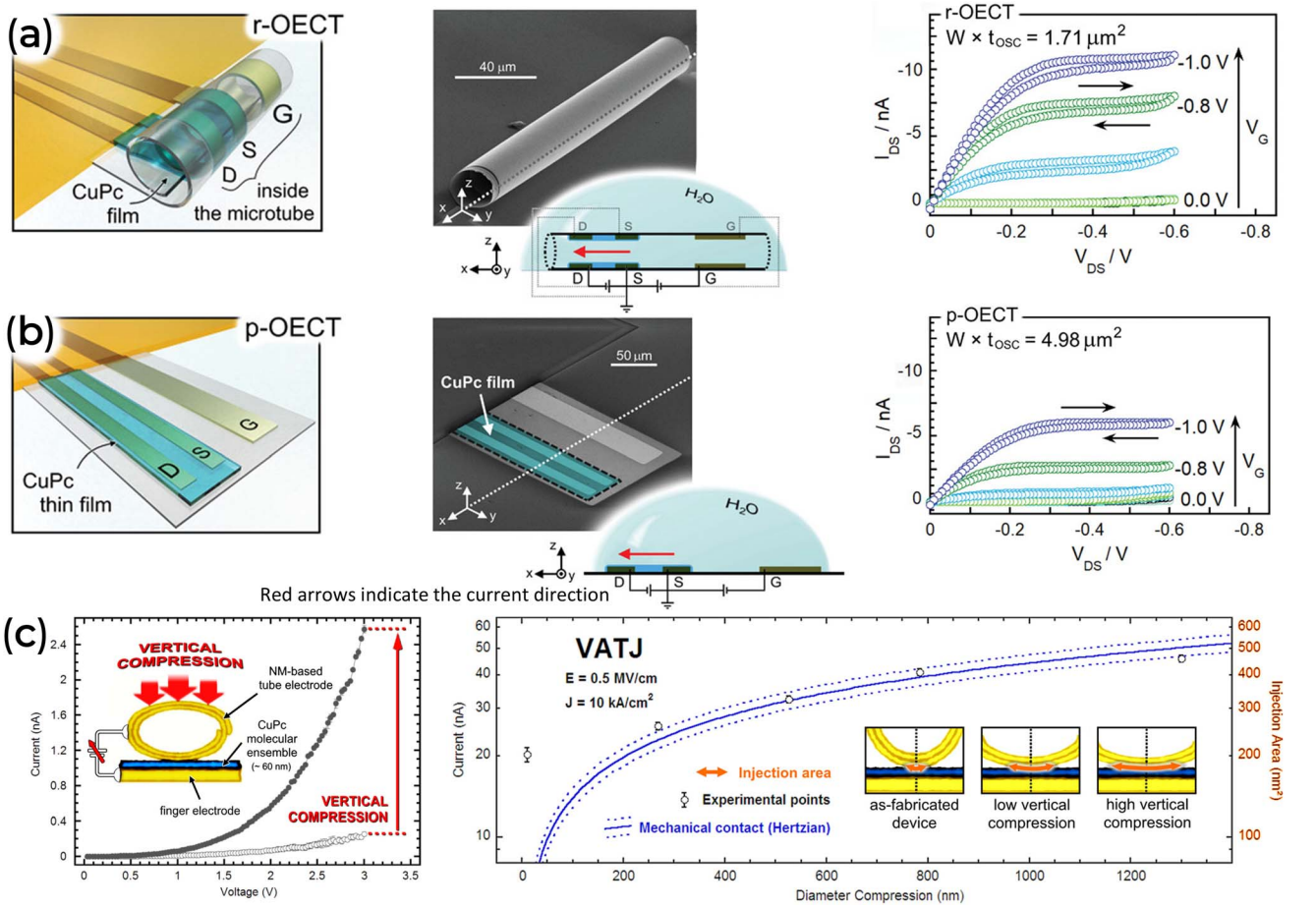


Fig. 17 (a) r-OECT and (b) p-OECT. (a and b) Represent each device configuration's sketches (left), SEM image (middle), and output curves (right). Adapted with permission from L. M. M. Ferro *et al.*[276] Copyright 2021, Wiley-VCH. (c) (Left) A lateral view of the VATJ and its electrical response before and under a vertical nanomembrane compression. (Right) Current and injection area as a function of nanomembrane diameter compression. Reprinted with permission from L. Merces, *et al.*[277] Copyright 2018, American Chemical Society.

electrical signals from multiple sensors into postsynaptic currents,[278] replicating the sensory reception, signal transmission, and processing functions of natural afferent nerves. As a result, VATJ systems hold promise for mimicking the behavior of a sensory nerve. Furthermore, they show great potential in next-generation wearable health monitors that track vital signs such as heart rate and respiration. These monitors provide real-time data to healthcare providers, aiding in the early detection of irregularities and enabling timely medical responses.

Strain-induced self-rolled-up nanomembranes also serve as a device platform for micro-supercapacitors (MSC) in personalized healthcare. Their ultrasmall volume and robust self-protection mechanical properties make them a cutting-edge solution for tiny, intravascular implants and microrobots operating within the human body.[279] Indeed, PEDOT-based tubular MSC achieved energy (7.73 μW h $cm^{-2}$) and power (17.8 mW $cm^{-2}$) densities and 94.1% capacitance retention after 5000 cycles,[280] which performs better than electrolytic capacitors.[281,282] The incorporation of PEDOT : PSS, a well-established biocompatible synthetic polymer, in these systems can eliminate the need for toxic or corrosive materials typically used in standard MSCs, ensuring complete biocompatibility for the tubular nano-biosupercapacitor (nBSC).[280] However, note that this device can still cause adverse reactions that are significantly higher than those caused by natural materials in biological environments (Fig. 11).

Interestingly, the intrinsic bioelectrocatalysis in blood can effectively counteract self-discharge tendencies, implying that blood can be directly used as an electrolyte to power autonomously implantable devices.[279,283] Additionally, using a PVA proton exchange separator enhances bioelectrocatalytic reactions in blood, effectively reducing self-discharge and improving overall device performance.[284,285] The nBSC delivers impressive specific capacitance, energy, and power densities and maintains significant retention of capacitance (~70%) and coulombic (~85%) efficiency over 5000 cycles.[283] These nBSCs are designed to operate stably in blood flow, avoiding gas evolution and withstanding various physiological pressures, such as the intricate dynamics within blood vessels, osmotic and hydrostatic pressures, and pressure-induced muscular contractions. Their robust structure offers radial flexibility and mechanical stability, which is crucial for intravascular implants.[279] Nonetheless, despite significant advancements, the energy storage capacity remains constrained.

## Summary and future inspirations

The next generation of biomedical and bioelectronics electronics needs to replace the current semiconductor-based electronics with a cognitive and adaptive high-performance computing capability to function fully. Neuromorphic devices (*i.e.*, devices with synapse-like functionalities) have the potential to be the best option for raison d'être. Therefore, this review presents natural materials for sustainable and wearable neuromorphic devices.

By mimicking the synaptic functionalities of the brain, natural biomaterials have demonstrated outstanding potential for logic operation, image and pattern recognition, implantable systems, and transient devices, making them candidates for future electronics. Specifically, we have shown that they can be assembled into 2-T and 3-T device structures without losing their biodegradability, biocompatibility, and mechanical features. Although we have presented a few examples of flexible devices and freestanding architectures, more detailed research on the stability and accuracy of synaptic properties on mechanical stress still needs to be completed. Moreover, up to now, there are a small number of neuromorphic sensors sensitive to light. Other external stimuli (*e.g.*, chemicals, pH, sound, temperature, touch, and pathogens) and biosignals are necessary studies that need to be addressed to expand the application of skin-attachable and implantable neuromorphic electronics for wearable computing and health monitoring. In such examples, the harsh conditions of the human body (or the surrounding environment) make encapsulation a matter of tremendous relevance to extend the lifetime of these devices.

Additionally, it requires decreasing power and energy consumption, improving performance homogeneity, and balancing the stability of the electrical and mechanical behavior to achieve efficient and stable artificial synaptic devices compatible with Nature. One realistic approach to reaching such a goal would be fabricating small devices that can alleviate the bending stress and allow excellent mechanical conformability. Nonetheless, the downscale can open technological dilemmas. For instance, the micro and nanoscale fabrication processes involve top-down lithographic methodologies, which use solid and toxic chemicals capable of negatively affecting soft materials (like natural ones), decreasing the eco-friendliness of the manufacturing process, and increasing harmful waste. Hence, it is usually considered an indirect strategy of multiple resists or solvent-less patterning methods that can result in complex fabrication protocol, lift-off feasibility, and, most importantly, poor resolution capabilities.[286–288] Fortunately, biomaterials also prove to have the ability to provide satisfactory technological advances for micro and nano geometric patterning approaches with fewer processing steps while being green.[289,290]

Under these circumstances, sustainable wearable artificial synapses require a combination of the fabrication process for smaller organic devices and their reliable synaptic abilities on biological tissue, natural environments, or building fabric without losing efficiency. Biocompatibility, minimal to no environmental footprint, and mechanical flexibility with low energy and power consumption (or even self-powered) are the fundamental principles for the functional (bio)materials to build such devices.

Another challenge associated with using this type of material is large-scale production and commercialization, as it could have high production costs associated with seasonal growth constraints and the need for specialized expertise or equipment to separate them from their natural source and remove any impurities or contaminants. Nevertheless, a few natural materials, such as shellac,[291,292] lignin,[293,294] and melanin,[209] are already being produced at large scales, offering a promising model for overcoming these limitations. A further solution to mitigate such

a rise in cost is to add an economic significance to what is commonly perceived as "waste" materials from the food and agricultural sectors.[31,264,295] For instance, by processing residues like corn stover, coffee grounds, fruit peels, and sugarcane bagasse, not only carbon-rich substances and natural extracts can be extracted and used in many other applications, but it also decreases the amount of incineration or improper disposal in unplanned landfills. On one side, advances in materials science and chemistry allow the optimization of the extraction and purification procedures of these materials, but could, on the other side, also offer an alternative to designing and engineering natural-inspired materials with the necessary properties to any specific needs.[31,252,296] The enhanced adaptability and customization of material properties can lead to the device's improved performance and efficiency.[209,252] A further consequence of adopting the synthetic approach is alleviating the exploitative and harmful practices associated with animal-based materials.[31]

The combination of natural organic biomaterial properties (environmentally benign, biodegradable, biocompatible, and featuring mechanical softness) with the ones from the memristors and electrolyte-gated transistors in a brain-inspired neuromorphic setup is a research theme that is in its infancy and far from large-scale practical applications. It cannot be denied today that there is a limited amount of work on the subject; however, it already shows a taste of the potential opportunity and diversity of applications. The fresh look displayed here unveils the association's power to become the coming wave of sustainable biomedical and bioelectronic technology.

## Data availability

No primary research results, software or code have been included and no new data were generated or analyzed as part of this review.

## Author contributions

J. V. Paulin: conceptualization, validation, investigation, writing—original draft, visualization. C. C. B. Bufon: writing—review and editing, supervision.

## Conflicts of interest

There are no conflicts to declare.

## Acknowledgements

The authors are thankful for the support of the São Paulo Research Foundation (FAPESP, grants: 2014/25979-2, 2020/15869-6 and 2023/09820-2). C. C. B. B. is a productivity Research Fellow from the Brazilian National Council for Scientific and Technological Development (CNPq grant 309011/2023-0). J. V. P. is also thankful for the support of FUNDUNESP and the São Paulo State University research office (PROPe) postdoctoral fellowship (05/2024).

## References

1 M. P. Cenci, T. Scarazzato, D. D. Munchen, P. C. Dartora, H. M. Veit, A. M. Bernardes and P. R. Dias, *Adv. Mater. Technol.*, 2022, **7**, 2001263.
2 J. Andreu-Perez, D. R. Leff, H. M. D. Ip and G. Z. Yang, *IEEE Trans. Biomed. Eng.*, 2015, **62**, 2750–2762.
3 M. S. Brown, B. Ashley and A. Koh, *Front. Bioeng. Biotechnol.*, 2018, **6**, 47.
4 X. Yu, W. Shou, B. K. Mahajan, X. Huang and H. Pan, *Adv. Mater.*, 2018, **30**, 1707624.
5 C. Choi, Y. Lee, K. W. Cho, J. H. Koo and D. H. Kim, *Acc. Chem. Res.*, 2019, **52**, 73–81.
6 W. B. Han, S. M. Yang, K. Rajaram and S. W. Hwang, *Adv. Sustainable Syst.*, 2022, **6**, 2100075.
7 National Academy of Engineering, *Grand Challenges for Engineering: Imperatives, Prospects, and Priorities: Summary of a Forum*, National Academies Press, Washington, DC, 2016, DOI: **10.17226/23440**.
8 H. C. Ates, P. Q. Nguyen, L. Gonzalez-Macia, E. Morales-Narváez, F. Güder, J. J. Collins and C. Dincer, *Nat. Rev. Mater.*, 2022, **7**, 887–907.
9 N. Kasabov, N. Sengupta and N. Scott, in *IEEE 8th International Conference on Intelligent Systems*, 2016, pp. 15–21.
10 H. T. Zhang, P. Panda, J. Lin, Y. Kalcheim, K. Wang, J. W. Freeland, D. D. Fong, S. Priya, I. K. Schuller, S. K. R. S. Sankaranarayanan, K. Roy and S. Ramanathan, *Appl. Phys. Rev.*, 2020, **7**, 011309.
11 S. Inal, J. Rivnay, A. O. Suiu, G. G. Malliaras and I. McCulloch, *Acc. Chem. Res.*, 2018, **51**, 1368–1376.
12 S. Dai, Y. Zhao, Y. Wang, J. Zhang, L. Fang, S. Jin, Y. Shao and J. Huang, *Adv. Funct. Mater.*, 2019, **29**, 1903700.
13 L. F. Abbott and W. G. Regehr, *Nature*, 2004, **431**, 796–803.
14 D. M. Kullmann and K. P. Lamsa, *Nat. Rev. Neurosci.*, 2007, **8**, 687–699.
15 C. Zamarreño-Ramos, L. A. Camuñas-Mesa, J. A. Perez-Carrasco, T. Masquelier, T. Serrano-Gotarredona and B. Linares-Barranco, *Front. Neurosci.*, 2011, **5**, 26.
16 A. E. Pereda, *Nat. Rev. Neurosci.*, 2014, **15**, 250–263.
17 X. Liu, F. Wang, J. Su, Y. Zhou and S. Ramakrishna, *Adv. Funct. Mater.*, 2022, **32**, 2113050.
18 A. Noy, *Adv. Mater.*, 2011, **23**, 807–820.
19 N. K. Upadhyay, H. Jiang, Z. Wang, S. Asapu, Q. Xia and J. Joshua Yang, *Adv. Mater. Technol.*, 2019, **4**, 1800589.
20 D. T. Simon, E. O. Gabrielsson, K. Tybrandt and M. Berggren, *Chem. Rev.*, 2016, **116**, 13009–13041.
21 Y. Lee and T. W. Lee, *Acc. Chem. Res.*, 2019, **52**, 964–974.
22 J. Zhu, T. Zhang, Y. Yang and R. Huang, *Appl. Phys. Rev.*, 2020, **7**, 011312.
23 H. L. Park, Y. Lee, N. Kim, D. G. Seo, G. T. Go and T. W. Lee, *Adv. Mater.*, 2020, **32**, 1903558.
24 14 Grand Challenges for Engineering in the 21st Century, **http://www.engineeringchallenges.org/challenges.aspx**, accessed 12 September 2023.
25 M. Irimia-Vladu, *Chem. Soc. Rev.*, 2014, **43**, 588–610.

26 J. Tropp and J. Rivnay, *J. Mater. Chem. C*, 2021, **9**, 13543–13556.
27 C. Santato and P. J. Alarco, *Adv. Mater. Technol.*, 2022, **7**, 2101265.
28 M. Chakraborty, J. Kettle and R. Dahiya, *IEEE J. Flex. Electron.*, 2022, **1**(1), 4–23, DOI: **10.1109/JFLEX.2022.3159258**.
29 Z. Lv, Y. Zhou, S. T. Han and V. A. L. Roy, *Mater. Today*, 2018, **21**, 537–552.
30 A. Tripathy, M. J. Nine, D. Losic and F. S. Silva, *Mater. Sci. Eng., R*, 2021, **146**, 100647.
31 J. V. Paulin and C. F. O. Graeff, *J. Mater. Chem. C*, 2021, **9**, 14514–14531.
32 M. J. Han and D. K. Yoon, *Engineering*, 2021, **7**, 564–580.
33 D. Gao, J. Lv and P. S. Lee, *Adv. Mater.*, 2022, **34**, 2105020.
34 F. Torricelli, I. Alessandri, E. Macchia, I. Vassalini, M. Maddaloni and L. Torsi, *Adv. Mater. Technol.*, 2022, **7**, 2100445.
35 Take Action for the Sustainable Development Goals – United Nations Sustainable Development, **https://www.un.org/sustainabledevelopment/sustainable-development-goals/**, accessed 12 September 2023.
36 S. Cohen-Cory, *Science*, 2002, **298**, 770–776.
37 *A Textbook of Neuroanatomy*, ed. M. A. Patestas and L. P. Gartner, John Wiley & Sons, 2016.
38 J. G. G. Borst and B. Sakmann, *Nature*, 1996, **383**, 431–434.
39 D. Kuzum, S. Yu and H. S. Philip Wong, *Nanotechnology*, 2013, **24**, 382001.
40 M. F. Bear and W. C. Abraham, *Annu. Rev. Neurosci.*, 1996, **19**, 437–462.
41 S. Royer and D. Paré, *Nature*, 2003, **422**, 518–522.
42 E. S. Fortune and G. J. Rose, *Trends Neurosci.*, 2001, **24**, 381–385.
43 R. S. Zucker and W. G. Regehr, *Annu. Rev. Physiol.*, 2002, **64**, 355–405.
44 T. V. P. Bliss and G. L. Collingridge, *Nature*, 1993, **361**, 31–39.
45 J. R. Whitlock, A. J. Heynen, M. G. Shuler and M. F. Bear, *Science*, 2006, **313**, 1093–1097.
46 G. Bornschein, O. Arendt, S. Hallermann, S. Brachtendorf, J. Eilers and H. Schmidt, *J. Physiol.*, 2013, **591**, 3355–3370.
47 S. L. Jackman, J. Turecek, J. E. Belinsky and W. G. Regehr, *Nature*, 2016, **529**, 88–91.
48 D. O. Hebb, *The Organization of Behavior: a Neuropsychological Theory*, Psychology Press, New York, 1st edn, 2002.
49 G. Q. Bi and M. M. Poo, *J. Neurosci.*, 1998, **18**, 10464–10472.
50 R. M. Harrison and M. Poole, *Neuron*, 2001, **32**, 1149–1164.
51 D. E. Feldman, *Neuron*, 2012, **75**, 556–571.
52 S. Saïghi, C. G. Mayr, T. Serrano-Gotarredona, H. Schmidt, G. Lecerf, J. Tomas, J. Grollier, S. Boyn, A. F. Vincent, D. Querlioz, S. La Barbera, F. Alibart, D. Vuillaume, O. Bichler, C. Gamrat and B. Linares-Barranco, *Front. Neurosci.*, 2015, **9**, 51.
53 S. M. Dudek and M. F. Bear, *Proc. Natl. Acad. Sci. U. S. A.*, 1992, **89**, 4363–4367.
54 Y. Van De Burgt, A. Melianas, S. T. Keene, G. Malliaras and A. Salleo, *Nat. Electron.*, 2018, **1**, 386–397.
55 Z. Huang, Y. Li, Y. Zhang, J. Chen, J. He and J. Jiang, *Int. J. Extreme Manuf.*, 2024, **6**, 032003.
56 D. Xie, Y. Li, J. He and J. Jiang, *Sci. China Mater.*, 2023, **66**, 4814–4824.
57 Y. Cheng, K. Shan, Y. Xu, J. Yang, J. He and J. Jiang, *Nanoscale*, 2020, **12**, 21798–21811.
58 Y. Park, M. K. Kim and J. S. Lee, *J. Mater. Chem. C*, 2020, **8**, 9163–9183.
59 F. Sun, Q. Lu, S. Feng and T. Zhang, *ACS Nano*, 2021, **15**, 3875–3899.
60 Y. Kim, J. S. An, D. Lee, S. Y. Ryu, Y. C. Hwang, D. H. Kim and T. W. Kim, *Sci. Rep.*, 2023, **13**, 6491.
61 T. Guo, J. Ge, B. Sun, K. Pan, Z. Pan, L. Wei, Y. Yan, Y. N. Zhou and Y. A. Wu, *Adv. Electron. Mater.*, 2022, **8**, 2200449.
62 L. Wang, Z. Zuo and D. Wen, *Adv. Biol.*, 2023, **7**, 2200298.
63 X. Yan, X. Li, Z. Zhou, J. Zhao, H. Wang, J. Wang, L. Zhang, D. Ren, X. Zhang, J. Chen, C. Lu, P. Zhou and Q. Liu, *ACS Appl. Mater. Interfaces*, 2019, **11**, 18654–18661.
64 L. Wang, T. Yang, Y. Ju and D. Wen, *Adv. Electron. Mater.*, 2023, 2300631, Early View, .
65 L. Wang, S. Wei, J. Xie, Y. Ju, T. Yang and D. Wen, *Nanomaterials*, 2023, **13**, 3012.
66 M. K. Kim and J. S. Lee, *ACS Nano*, 2018, **12**, 1680–1687.
67 K. Zhang, Q. Xue, C. Zhou, W. Mo, C. C. Chen, M. Li and T. Hang, *Nanoscale*, 2022, **14**, 12898–12908.
68 J. Ge, D. Li, C. Huang, X. Zhao, J. Qin, H. Liu, W. Ye, W. Xu, Z. Liu and S. Pan, *Nanoscale*, 2020, **12**, 720–730.
69 T. Hussain, H. Abbas, C. Youn, H. Lee, T. Boynazarov, B. Ku, Y. R. Jeon, H. Han, J. H. Lee, C. Choi and T. Choi, *Adv. Mater. Technol.*, 2022, **7**, 2100744.
70 T. R. Desai, S. S. Kundale, T. D. Dongale and C. Gurnani, *ACS Appl. Bio Mater.*, 2023, **6**, 1763–1773.
71 L. Wang, S. Wei, J. Xie and D. Wen, *ACS Sustain. Chem. Eng.*, 2023, **11**, 2229–2237.
72 P. Jetty, D. P. Sahu and S. Jammalamadaka, *Phys. Status Solidi RRL*, 2022, **16**, 2100465.
73 J. G. Min and W. J. Cho, *Micromachines*, 2021, **12**, 1259.
74 S. Y. Min and W. J. Cho, *Int. J. Mol. Sci.*, 2021, **22**, 773.
75 N. Raeis-Hosseini, Y. Park and J. S. Lee, *Adv. Funct. Mater.*, 2018, **28**, 1800553.
76 D. H. Kang, J. H. Kim, S. Oh, H. Y. Park, S. R. Dugasani, B. S. Kang, C. Choi, R. Choi, S. Lee, S. H. Park, K. Heo and J. H. Park, *Adv. Sci.*, 2019, **6**, 1901265.
77 Y. C. Lin, T. H. Hsiao, Y. T. Li, L. Di Huang, L. Fruk and Y. C. Hung, *Org. Electron.*, 2023, **114**, 106745.
78 B. Sueoka, K. Y. Cheong and F. Zhao, *Appl. Phys. Lett.*, 2022, **120**, 083301.
79 B. Sueoka and F. Zhao, *J. Phys. D Appl. Phys.*, 2022, **55**, 225105.
80 B. Sueoka, M. Hasan, L. Williams, Z. Xiao, Y. Zhi, K. Yew and F. Zhao, *Org. Electron.*, 2022, **109**, 106622.
81 J. H. Lee, Y. S. Rim, W. K. Min, K. Park, H. T. Kim, G. Hwang, J. Song and H. J. Kim, *Adv. Funct. Mater.*, 2021, **31**, 2107074.

82 C. Shi, J. Lan, J. Wang, S. Zhang, Y. Lin, S. Zhu, A. E. Stegmann, R. Yu, X. Yan and X. Y. Liu, *Adv. Funct. Mater.*, 2020, **30**, 2002882.
83 Y. Park and J. S. Lee, *ACS Nano*, 2017, **11**, 8962–8969.
84 Y. Sun, Q. Yuan, Y. Wang, B. Li and D. Wen, *ACS Sustain. Chem. Eng.*, 2023, **11**, 15710–15720.
85 J. G. Min, H. Park and W. J. Cho, *Nanomaterials*, 2022, **12**, 2978.
86 T. Fu, X. Liu, H. Gao, J. E. Ward, X. Liu, B. Yin, Z. Wang, Y. Zhuo, D. J. F. Walker, J. Joshua Yang, J. Chen, D. R. Lovley and J. Yao, *Nat. Commun.*, 2020, **11**, 1861.
87 D. H. Choi, H. T. Kim, Y. Kim, K. Park, M. S. Kim, J. H. Lee, G. I. Kim, J. J. Chung and H. J. Kim, *Appl. Surf. Sci.*, 2023, **621**, 156814.
88 L. Wang, H. Zhu and D. Wen, *J. Phys. Chem. Lett.*, 2021, **12**, 8956–8962.
89 C. Shi, J. Wang, M. L. Sushko, W. Qiu, X. Yan and X. Y. Liu, *Adv. Funct. Mater.*, 2019, **29**, 1904777.
90 M. Zhao, S. Wang, D. Li, R. Wang, F. Li, M. Wu, K. Liang, H. Ren, X. Zheng, C. Guo, X. Ma, B. Zhu, H. Wang and Y. Hao, *Adv. Electron. Mater.*, 2022, **8**, 2101139.
91 Y. Xing, C. Shi, J. Zhao, W. Qiu, N. Lin, J. Wang, X. B. Yan, W. D. Yu and X. Y. Liu, *Small*, 2017, **13**, 1702390.
92 J. Wang, C. Shi, M. L. Sushko, J. Lan, K. Sun, J. Zhao, X. Liu and X. Yan, *ACS Appl. Mater. Interfaces*, 2021, **13**, 39641–39651.
93 M. Y. Chougale, M. U. Khan, J. Kim, R. A. Shaukat, Q. M. Saqib, S. R. Patil, T. D. Dongale, A. Bermak, B. Mohammad and J. Bae, *Adv. Eng. Mater.*, 2022, **2200314**, 1–9.
94 S. Liu, Y. Cheng, F. Han, S. Fan and Y. Zhang, *Chem. Eng. J.*, 2023, **471**, 144678.
95 L. Wang, W. Li and D. Wen, *J. Alloys Compd.*, 2023, **953**, 170119.
96 L. Wang, W. Li and D. Wen, *Microelectron. Eng.*, 2023, **267–268**, 111911.
97 E. Zhao, J. Jiang, G. Liu, C. Wang, C. Zhou and Z. Zhang, *J. Mater. Sci.: Mater. Electron.*, 2023, **34**, 1688.
98 L. Wang, J. Li and D. Wen, *ACS Appl. Electron. Mater.*, 2023, **5**, 397–405.
99 B. Sun, Y. Chen, G. Zhou, Y. Zhou, T. Guo, S. Zhu, S. Mao, Y. Zhao, J. Shao and Y. Li, *Adv. Electron. Mater.*, 2023, **9**, 2201017.
100 T. R. Desai, T. D. Dongale, S. R. Patil, A. P. Tiwari, P. K. Pawar, R. K. Kamat and T. G. Kim, *J. Mater. Res. Technol.*, 2021, **11**, 1100–1110.
101 Y. Kim, C. H. Park, J. S. An, S. H. Choi and T. W. Kim, *Sci. Rep.*, 2021, **11**, 20633.
102 L. Chua, *Semicond. Sci. Technol.*, 2014, **29**, 104001.
103 S. Goswami, S. Goswami and T. Venkatesan, *Appl. Phys. Rev.*, 2020, **7**, 021303.
104 G. Zhou, Z. Wang, B. Sun, F. Zhou, L. Sun, H. Zhao, X. Hu, X. Peng, J. Yan, H. Wang, W. Wang, J. Li, B. Yan, D. Kuang, Y. Wang, L. Wang and S. Duan, *Adv. Electron. Mater.*, 2022, **8**, 2101127.
105 J. Wang, S. Mao, S. Zhu, W. Hou, F. Yang and B. Sun, *Org. Electron.*, 2022, **106**, 106540.
106 C. Baeumer, N. Raab, T. Menke, C. Schmitz, R. Rosezin, P. Müller, M. Andrä, V. Feyer, R. Bruchhaus, F. Gunkel, C. M. Schneider, R. Waser and R. Dittmann, *Nanoscale*, 2016, **8**, 13967–13975.
107 R. Yang, H. M. Huang, Q. H. Hong, X. B. Yin, Z. H. Tan, T. Shi, Y. X. Zhou, X. S. Miao, X. P. Wang, S. B. Mi, C. L. Jia and X. Guo, *Adv. Funct. Mater.*, 2018, **28**, 1704455.
108 Y. Lin, T. Zeng, H. Xu, Z. Wang, X. Zhao, W. Liu, J. Ma and Y. Liu, *Adv. Electron. Mater.*, 2018, **4**, 1800373.
109 N. R. Hosseini and J. S. Lee, *Adv. Funct. Mater.*, 2015, **25**, 5586–5592.
110 M. K. Choi, W. K. Kim, S. Sung, C. Wu, H. W. Kim and T. W. Kim, *Sci. Rep.*, 2018, **8**, 12275.
111 S. R. Zhang, L. Zhou, J. Y. Mao, Y. Ren, J. Q. Yang, G. H. Yang, X. Zhu, S. T. Han, V. A. L. Roy and Y. Zhou, *Adv. Mater. Technol.*, 2019, **4**, 1800342.
112 D. Kuzum, R. G. D. Jeyasingh, B. Lee and H.-S. P. Wong, *Nano Lett.*, 2012, **12**, 2179–2186.
113 L. Wang, S. R. Lu and J. Wen, *Nanoscale Res. Lett.*, 2017, **12**, 347.
114 S. Il Kim, Y. Lee, M. H. Park, G. T. Go, Y. H. Kim, W. Xu, H. D. Lee, H. Kim, D. G. Seo, W. Lee and T. W. Lee, *Adv. Electron. Mater.*, 2019, **5**, 1900008.
115 L. Q. Guo, Z. Y. Li, L. Q. Zhu, Z. Y. Ren, H. Xiao and J. C. Cai, *Org. Electron.*, 2020, **87**, 105961.
116 G. Wu, P. Feng, X. Wan, L. Zhu, Y. Shi and Q. Wan, *Sci. Rep.*, 2016, **6**, 23578.
117 H. Kim, H. Park and W.-J. Cho, *Nanomaterials*, 2022, **12**, 2596.
118 S. Dai, Y. Wang, J. Zhang, Y. Zhao, F. Xiao, D. Liu, T. Wang and J. Huang, *ACS Appl. Mater. Interfaces*, 2018, **10**, 39983–39991.
119 J. Zhang, D. Liu, Q. Shi, B. Yang, P. Guo, L. Fang, S. Dai, L. Xiong and J. Huang, *npj Flexible Electron.*, 2022, **6**, 30.
120 W. S. Wang, Z. W. Shi, X. L. Chen, Y. Li, H. Xiao, Y. H. Zeng, X. D. Pi and L. Q. Zhu, *ACS Appl. Mater. Interfaces*, 2023, **15**, 47640–47648.
121 Y. Li, L. Jing, X. Xiong, R. Tao, Z. Fan, X. Lu, G. Zhou, Z. Fang, H. Ning and J. Liu, *Surf. Interfaces*, 2024, **44**, 103666.
122 M. J. Han and V. V. Tsukruk, *ACS Nano*, 2023, **17**, 18883–18892.
123 F. Yu, L. Q. Zhu, H. Xiao, W. T. Gao and Y. B. Guo, *Adv. Funct. Mater.*, 2018, **28**, 1804025.
124 J. Chen, E. Li, Y. Yan, Q. Yang, S. Cao, J. Zhong, H. Chen and T. Guo, *J. Phys. D Appl. Phys.*, 2019, **52**, 484002.
125 W. Hu, J. Jiang, D. Xie, B. Liu, J. Yang and J. He, *J. Mater. Chem. C*, 2019, **7**, 682–691.
126 G. Wu, J. Zhang, X. Wan, Y. Yang and S. Jiang, *J. Mater. Chem. C*, 2014, **2**, 6249–6255.
127 Y. H. Liu, L. Q. Zhu, P. Feng, Y. Shi and Q. Wan, *Adv. Mater.*, 2015, **27**, 5599–5604.
128 D. H. Lee, H. S. Kim, K. W. Park, H. Park and W. J. Cho, *Biomimetics*, 2023, **8**, 432.
129 D. H. Lee, H. Park and W. J. Cho, *Gels*, 2023, **9**, 931.
130 Q. Ou, B. Yang, J. Zhang, D. Liu, T. Chen, X. Wang, D. Hao, Y. Lu and J. Huang, *Small*, 2021, **17**, 2007241.

131 B. Yang, Y. Lu, D. Jiang, Z. Li, Y. Zeng, S. Zhang, Y. Ye, Z. Liu, Q. Ou, Y. Wang, S. Dai, Y. Yi and J. Huang, *Adv. Mater.*, 2020, **32**, 2001227.
132 Y. Yang, X. Zhao, C. Zhang, Y. Tong, J. Hu, H. Zhang, M. Yang, X. Ye, S. Wang, Z. Sun, Q. Tang and Y. Liu, *Adv. Funct. Mater.*, 2020, **30**, 2006271.
133 Y. Yang, X. Zhao, S. Wang, C. Zhang, H. Sun, F. Xu, Y. Tong, Q. Tang and Y. Liu, *J. Mater. Chem. C*, 2020, **8**, 16542–16550.
134 T. Nguyen-dang, K. Harrison, A. Lill, A. Dixon, E. Lewis, J. Vollbrecht, T. Hachisu, S. Biswas, Y. Visell and T. Nguyen, *Adv. Electron. Mater.*, 2021, **7**, 2100519.
135 J. Ko, L. T. H. Nguyen, A. Surendran, B. Y. Tan, K. W. Ng and W. L. Leong, *ACS Appl. Mater. Interfaces*, 2017, **9**, 43004–43012.
136 W. Qin, B. H. Kang and H. J. Kim, *ACS Appl. Mater. Interfaces*, 2021, **13**, 34597–34604.
137 H. Qiu, D. Hao, H. Li, Y. Shi, Y. Dong, G. Liu and F. Shan, *Appl. Phys. Lett.*, 2022, **121**, 183301.
138 S. H. Kim and W. J. Cho, *Polymers*, 2022, **14**, 1372.
139 Y. Li, C. Zhang, X. Zhao, Y. Tong, Q. Tang and Y. Liu, *ACS Appl. Electron. Mater.*, 2022, **4**, 316–325.
140 C. Zhang, F. Xu, X. Zhao, M. Zhang, W. Han, H. Yu, S. Wang, Y. Yang, Y. Tong, Q. Tang and Y. Liu, *Nano Energy*, 2022, **95**, 107001.
141 J. Wen, L. Q. Zhu, H. F. Qi, Z. Y. Ren, F. Wang and H. Xiao, *Org. Electron.*, 2020, **82**, 105782.
142 S. Kazemzadeh, L. Dodsworth, I. F. Pereira, Y. Van De Burgt, F. Pereira and Y. Van De Burgt, *Adv. Electron. Mater.*, 2023, **9**, 2200427.
143 X. Han, J. Zhang, T. Zeng, X. Zhao, J. Li, H. Sun, Y. Cao, Y. Tong, Q. Tang and Y. Liu, *IEEE Electron Device Lett.*, 2023, **44**, 606–609.
144 Z. Lv, M. Chen, F. Qian, V. A. L. Roy, W. Ye, D. She, Y. Wang, Z. X. Xu, Y. Zhou and S. T. Han, *Adv. Funct. Mater.*, 2019, **29**, 1902374.
145 W. Hu, J. Jiang, D. Xie, S. Wang, K. Bi, H. Duan, J. Yang and J. He, *Nanoscale*, 2018, **10**, 14893–14901.
146 Y. Li, K. Yin, Y. Diao, M. Fang, J. Yang, J. Zhang, H. Cao, X. Liu and J. Jiang, *Nanoscale*, 2022, **14**, 2316–2326.
147 H. Choi, Y. Lee, H. Park and W.-J. Cho, *Int. J. Mol. Sci.*, 2022, **23**, 15901.
148 L. Q. Guo, J. Tao, L. Q. Zhu, H. Xiao, W. T. Gao, F. Yu and Y. M. Fu, *Org. Electron.*, 2018, **61**, 312–317.
149 F. Torricelli, D. Z. Adrahtas, Z. Bao, M. Berggren, F. Biscarini, A. Bonfiglio, C. A. Bortolotti, C. D. Frisbie, E. Macchia, G. G. Malliaras, I. McCulloch, M. Moser, T.-Q. Nguyen, R. M. Owens, A. Salleo, A. Spanu and L. Torsi, *Nat. Rev. Methods Primers*, 2021, **1**, 66.
150 M. Jin, H. Lee, C. Im, H. J. Na, J. H. Lee, W. H. Lee, J. Han, E. Lee, J. Park and Y. S. Kim, *Adv. Funct. Mater.*, 2022, **32**, 2201048.
151 D. Xie, X. Liang, D. Geng, Q. Wu and C. Liu, *Electronics*, 2024, **13**, 1485.
152 F. Yu, F. Yu, F. Yu, J. C. Cai, J. C. Cai, J. C. Cai, L. Q. Zhu, L. Q. Zhu, M. Sheikhi, M. Sheikhi, Y. H. Zeng, Y. H. Zeng, W. Guo, W. Guo, Z. Y. Ren, Z. Y. Ren, H. Xiao, H. Xiao, J. C. Ye, J. C. Ye, C. H. Lin, A. B. Wong and T. Wu, *ACS Appl. Mater. Interfaces*, 2020, **12**, 26258–26266.
153 X. Liu, C. Sun, Z. Guo, Y. Zhang, Z. Zhang, J. Shang, Z. Zhong, X. Zhu, X. Yu and R. W. Li, *Nanoscale Adv.*, 2022, **4**, 2412–2419.
154 L. Q. Guo, H. Han, L. Q. Zhu, Y. B. Guo, F. Yu, Z. Y. Ren, H. Xiao, Z. Y. Ge and J. N. Ding, *ACS Appl. Mater. Interfaces*, 2019, **11**, 28352–28358.
155 Y. Zhu, G. Liu, Z. Xin, C. Fu, Q. Wan and F. Shan, *ACS Appl. Mater. Interfaces*, 2020, **12**, 1061–1068.
156 Y. M. Fu, H. Li, T. Wei, L. Huang, F. Hidayati and A. Song, *ACS Appl. Electron. Mater.*, 2022, **4**, 2933–2942.
157 S. Jang, S. Jang, E. H. Lee, M. Kang, G. Wang and T. W. Kim, *ACS Appl. Mater. Interfaces*, 2019, **11**, 1071–1080.
158 Q. Zhang, T. Jin, X. Ye, D. Geng, W. Chen and W. Hu, *Adv. Funct. Mater.*, 2021, **31**, 2106151.
159 K. Sun, J. Chen and X. Yan, *Adv. Funct. Mater.*, 2021, **31**, 2006773.
160 I. Segev and I. Parnas, *Biophys. J.*, 1983, **41**, 41–50.
161 P. Béguin and J.-P. Aubert, *FEMS Microbiol. Rev.*, 1994, **13**, 25–58.
162 V. R. Feig, H. Tran and Z. Bao, *ACS Cent. Sci.*, 2018, **4**, 337–348.
163 R. Singh, M. J. Bathaei, E. Istif and L. Beker, *Adv. Healthcare Mater.*, 2020, **9**, 2000790.
164 U. Sharma, D. Concagh, L. Core, Y. Kuang, C. You, Q. Pham, G. Zugates, R. Busold, S. Webber, J. Merlo, R. Langer, G. M. Whitesides and M. Palasis, *Nat. Mater.*, 2018, **17**, 96–102.
165 M. Irimia-vladu and N. S. Sariciftci, *Polym. Int.*, 2024, DOI: **10.1002/pi.6697**Early View.
166 S. K. Kang, J. Koo, Y. K. Lee and J. A. Rogers, *Acc. Chem. Res.*, 2018, **51**, 988–998.
167 J. S. Shim, J. A. Rogers and S. K. Kang, *Mater. Sci. Eng., R*, 2021, **145**, 100624.
168 L. Ceseracciu, J. A. Heredia-guerrero, S. Dante, A. Athanassiou and I. S. Bayer, *ACS Appl. Mater. Interfaces*, 2015, **7**, 3742–3753.
169 M. Baumgartner, F. Hartmann, M. Drack, D. Preninger, D. Wirthl, R. Gerstmayr, L. Lehner, G. Mao, R. Pruckner, S. Demchyshyn, L. Reiter, M. Strobel, T. Stockinger, D. Schiller, S. Kimeswenger, F. Greibich, G. Buchberger, E. Bradt, S. Hild, S. Bauer and M. Kaltenbrunner, *Nat. Mater.*, 2020, **19**, 1102–1109.
170 M. Santhiago, P. G. Da Costa, M. P. Pereira, C. C. Corrêa, V. B. De Morais and C. C. B. Bufon, *ACS Appl. Mater. Interfaces*, 2018, **10**, 35631–35638.
171 A. C. Fingolo, V. B. de Morais, S. V. Costa, C. C. Corrêa, B. Lodi, M. Santhiago, J. S. Bernardes and C. C. B. Bufon, *ACS Appl. Bio Mater.*, 2021, **4**, 6682–6689.
172 C. Shi, F. Hu, R. Wu, Z. Xu, G. Shao, R. Yu and X. Y. Liu, *Adv. Mater.*, 2021, **33**, 2005910.
173 M. Stoppa and A. Chiolerio, *Sensors*, 2014, **14**, 11957–11992.
174 Y. Lee, J. Y. Oh, W. Xu, O. Kim, T. R. Kim, J. Kang, Y. Kim, D. Son, J. B. H. Tok, M. J. Park, Z. Bao and T. W. Lee, *Sci. Adv.*, 2018, **4**, eaat7387.

175 Y. R. Jeong, G. Lee, H. Park and J. S. Ha, *Acc. Chem. Res.*, 2019, **52**, 91–99.
176 L. Liu and X. Zhang, *Micromachines*, 2022, **13**, 1356.
177 G. Lee, M. Zarei, Q. Wei, Y. Zhu and S. G. Lee, *Small*, 2022, **18**, 2203491.
178 T. Yamada, Y. Hayamizu, Y. Yamamoto, Y. Yomogida, A. Izadi-Najafabadi, D. N. Futaba and K. Hata, *Nat. Nanotechnol.*, 2011, **6**, 296–301.
179 S. Bauer, S. Bauer-Gogonea, I. Graz, M. Kaltenbrunner, C. Keplinger and R. Schwödiauer, *Adv. Mater.*, 2014, **26**, 149–162.
180 Y. Qiu, E. Zhang, R. Plamthottam and Q. Pei, *Acc. Chem. Res.*, 2019, **52**, 316–325.
181 Y. Song, P. Li, M. Li, H. Li, C. Li, D. Sun and B. Yang, *Mater. Sci. Eng., C*, 2017, **79**, 740–747.
182 J. Y. Kim, Y. J. Yun, J. Jeong, C. Yoon Kim, K. R. Möller and S. W. Lee, *Sci. Adv.*, 2021, **7**, eabe7432.
183 C. Wang, H. Wang, B. Wang, H. Miyata, Y. Wang, M. O. G. Nayeem, J. J. Kim, S. Lee, T. Yokota, H. Onodera and T. Someya, *Sci. Adv.*, 2022, **8**, eabo1396.
184 B. C. Kang and T. J. Ha, *Appl. Phys. Lett.*, 2022, **120**, 213301.
185 J. W. Seo, H. Kim, K. H. Kim, S. Q. Choi and H. J. Lee, *Adv. Funct. Mater.*, 2018, **28**, 1800802.
186 Q. Wang, S. Ling, X. Liang, H. Wang, H. Lu and Y. Zhang, *Adv. Funct. Mater.*, 2019, **29**, 1808695.
187 Q. Li, G. Chen, Y. Cui, S. Ji, Z. Liu, C. Wan, Y. Liu, Y. Lu, C. Wang, N. Zhang, Y. Cheng, K. Q. Zhang and X. Chen, *ACS Nano*, 2021, **15**, 9955–9966.
188 L. Meng, Q. Fu, S. Hao, F. Xu and J. Yang, *Chem. Eng. J.*, 2022, **427**, 131999.
189 J. Cheng, L. You, X. Cai, J. Yang, H. Chen, X. Shi, J. Wu, J. Wang, C. Xiong and S. Wang, *ACS Appl. Mater. Interfaces*, 2022, **14**, 26338–26349.
190 H. Liu, W. Wei, L. Zhang, J. Xiao, J. Pan, Q. Wu, S. Ma, H. Dong, L. Yu, W. Yang, D. Wei, H. Ouyang and Y. Liu, *Adv. Funct. Mater.*, 2021, **31**, 2104088.
191 D. Song, G. Ye, Y. Zhao, Y. Zhang, X. Hou and N. Liu, *ACS Nano*, 2022, **16**, 17168–17178.
192 X. Liang, M. Zhu, H. Li, J. Dou, M. Jian, K. Xia, S. Li and Y. Zhang, *Adv. Funct. Mater.*, 2022, **32**, 2200162.
193 S. Shi, Y. Wang, Q. Meng, Z. Lan, C. Liu, Z. Zhou, Q. Sun and X. Shen, *ACS Appl. Mater. Interfaces*, 2023, **15**, 1903–1913.
194 G. D. Spyropoulos, J. N. Gelinas and D. Khodagholy, *Sci. Adv.*, 2019, **5**, eaau7378.
195 P. Meredith, C. J. Bettinger, M. Irimia-Vladu, A. B. Mostert and P. E. Schwenn, *Rep. Prog. Phys.*, 2013, **76**, 034501.
196 E. R. W. Van Doremaele, P. Gkoupidenis and Y. Van De Burgt, *J. Mater. Chem. C*, 2019, **7**, 12754–12760.
197 Z. Julier, A. J. Park, P. S. Briquez and M. M. Martino, *Acta Biomater.*, 2017, **53**, 13–28.
198 B. Ferrigno, R. Bordett, N. Duraisamy, J. Moskow, M. R. Arul, S. Rudraiah, S. P. Nukavarapu, A. T. Vella and S. G. Kumbar, *Bioact. Mater.*, 2020, **5**, 468–485.
199 J. H. Lee, P. Parthiban, G. Z. Jin, J. C. Knowles and H. W. Kim, *Prog. Mater. Sci.*, 2021, **117**, 100732.
200 M. Liu, Y. Zhang, Y. Zhang, Z. Zhou, N. Qin and T. H. Tao, *Adv. Sci.*, 2022, **9**, 2102596.
201 J. Liu, J. Chen, F. Dai, J. Zhao, S. Li, Y. Shi, W. Li, L. Geng, M. Ye, X. Chen, Y. Liu and W. Guo, *Nano Energy*, 2022, **103**, 107764.
202 Y. Long, J. Li, F. Yang, J. Wang and X. Wang, *Adv. Sci.*, 2021, **8**, 2004023.
203 R. Magisetty and S. M. Park, *Micromachines*, 2022, **13**, 161.
204 J. P. Evans and C. K. Sen, *Bioengineering*, 2023, **10**, 711.
205 E. Donati and G. Indiveri, *Prog. Biomed. Eng.*, 2023, **5**, 013002.
206 J. Lv, J. Chen and P. S. Lee, *SusMat*, 2021, **1**, 285–302.
207 S. Dalwadi, A. Goel, C. Kapetanakis, D. Salas-de la Cruz and X. Hu, *Int. J. Mol. Sci.*, 2023, **24**, 3975.
208 S. Ahmed, P. Sharma, S. Bairagi, N. P. Rumjit, S. Garg, A. Ali, C. W. Lai, S. M. Mousavi, S. A. Hashemi and C. M. Hussain, *J. Energy Storage*, 2023, **66**, 107391.
209 J. V. Paulin, *RSC Sustainability*, 2024, **2**, 2190–2198.
210 S. Dubey and A. Roulin, *Pigm. Cell Melanoma Res.*, 2014, **27**, 327–338.
211 M. M. Jastrzebska, H. Isotalo, J. Paloheimo and H. Stubb, *J. Biomater. Sci., Polym. Ed.*, 1995, **7**, 577–586.
212 A. B. Mostert, B. J. Powell, F. L. Pratt, G. R. Hanson, T. Sarna, I. R. Gentle and P. Meredith, *Proc. Natl. Acad. Sci. U. S. A.*, 2012, **109**, 8943–8947.
213 J. V. Paulin, A. P. Coleone, A. Batagin-Neto, G. Burwell, P. Meredith, C. F. O. Graeff and A. B. Mostert, *J. Mater. Chem. C*, 2021, **9**, 8345–8358.
214 J. V. Paulin, M. P. Pereira, B. A. Bregadiolli, J. P. Cachaneski-Lopes, C. F. O. Graeff and C. C. B. Bufon, *J. Mater. Chem. C*, 2023, **11**, 6107–6118.
215 J. Wünsche, Y. Deng, P. Kumar, E. Di Mauro, E. Josberger, J. Sayago, A. Pezzella, F. Soavi, F. Cicoira, M. Rolandi and C. Santato, *Chem. Mater.*, 2015, **27**, 436–442.
216 M. Sheliakina, A. B. Mostert and P. Meredith, *Adv. Funct. Mater.*, 2018, **28**, 1805514.
217 K. A. Motovilov, V. Grinenko, M. Savinov, Z. V. Gagkaeva, L. S. Kadyrov, A. A. Pronin, Z. V. Bedran, E. S. Zhukova, A. B. Mostert and B. P. Gorshunov, *RSC Adv.*, 2019, **9**, 3857–3867.
218 P. Kumar, E. Di Mauro, S. Zhang, A. Pezzella, F. Soavi, C. Santato and F. Cicoira, *J. Mater. Chem. C*, 2016, **4**, 9516–9525.
219 Z. Tehrani, S. P. Whelan, B. Mostert, J. V. Paulin, M. M. Ali, E. D. Ahmadi, C. F. de O. Graeff, O. J. Guy and D. T. Gethin, *2D Mater.*, 2020, **7**, 024008.
220 M. Piacenti-Silva, J. C. Fernandes, N. B. de Figueiredo, M. Congiu, M. Mulato and C. F. de O. Graeff, *AIP Adv.*, 2014, **4**, 037120.
221 M. Sheliakina, A. B. Mostert and P. Meredith, *Mater. Horiz.*, 2018, **5**, 256–263.
222 M. Ambrico, A. Cardone, T. Ligonzo, V. Augelli, P. F. Ambrico, S. Cicco, G. M. Farinola, M. Filannino, G. Perna and V. Capozzi, *Org. Electron.*, 2010, **11**, 1809–1814.

223 M. Ambrico, P. F. Ambrico, T. Ligonzo, A. Cardone, S. R. Cicco, A. Lavizzera, V. Augelli and G. M. Farinola, *Appl. Phys. Lett.*, 2012, **100**, 253702.
224 J. Wünsche, L. Cardenas, F. Rosei, F. Cicoira, R. Gauvin, C. F. O. Graeff, S. Poulin, A. Pezzella and C. Santato, *Adv. Funct. Mater.*, 2013, **23**, 5591–5598.
225 E. Di Mauro, O. Carpentier, S. I. Yáñez Sánchez, N. Ignoumba Ignoumba, M. Lalancette-Jean, J. Lefebvre, S. Zhang, C. F. O. Graeff, F. Cicoira and C. Santato, *J. Mater. Chem. C*, 2016, **4**, 9544–9553.
226 R. Xu, A. Gouda, M. F. Caso, F. Soavi and C. Santato, *ACS Omega*, 2019, **4**, 12244–12251.
227 Y. J. Kim, W. Wu, S. Chun, J. F. Whitacre and C. J. Bettinger, *Proc. Natl. Acad. Sci. U. S. A.*, 2013, **110**, 20912–20917.
228 Y. J. Kim, W. Wu, S. E. Chun, J. F. Whitacre and C. J. Bettinger, *Adv. Mater.*, 2014, **26**, 6572–6579.
229 J. V. Paulin, S. L. Fernandes and C. F. O. Graeff, *Electrochem*, 2021, **2**, 264–273.
230 C. J. Bettinger, *Trends Biotechnol.*, 2015, **33**, 575–585.
231 C. J. Bettinger, J. P. Bruggeman, A. Misra, J. T. Borenstein and R. Langer, *Biomaterials*, 2009, **30**, 3050–3057.
232 M. Piacenti-Silva, A. A. Matos, J. V. Paulin, R. A. da S. Alavarce, R. C. de Oliveira and C. F. Graeff, *Polym. Int.*, 2016, **65**, 1347–1354.
233 T. Eom, J. Jeon, S. Lee, K. Woo, J. E. Heo, D. C. Martin, J. J. Wie and B. S. Shim, *Part. Part. Syst. Charact.*, 2019, **36**, 1900166.
234 E. Di Mauro, D. Rho and C. Santato, *Nat. Commun.*, 2021, **12**, 3167.
235 N. Gogurla, B. Roy, K. Min, J. Y. Park and S. Kim, *Adv. Mater. Technol.*, 2020, **5**, 1900936.
236 S. P. Whelan, Z. Tehrani, M. Peacock, J. V. Paulin, O. Guy and D. Gethin, *J. Electroanal. Chem.*, 2022, **904**, 115868.
237 X. Zhang, Y. Peng, X. Wang and R. Ran, *ACS Appl. Polym. Mater.*, 2021, **3**, 1899–1911.
238 N. Contreras-Pereda, S. Suárez-García, R. Pfattner and D. Ruiz-Molina, *Mater. Today Chem.*, 2024, **35**, 101855.
239 A. Wahab, N. Gogurla, J. Y. Park and S. Kim, *Adv. Mater. Technol.*, 2022, **7**, 2101271.
240 J. V. Paulin, L. G. S. Albano, D. H. S. Camargo, M. P. Pereira, B. A. Bregadiolli, C. F. O. Graeff and C. C. B. Bufon, *Appl. Mater. Today*, 2022, **28**, 101525.
241 N. Gogurla, A. Wahab and S. Kim, *Mater. Today Bio*, 2023, **20**, 100642.
242 N. L. Nozella, J. V. M. Lima, R. F. de Oliveira and C. F. de O. Graeff, *Mater. Adv.*, 2023, **4**, 4732–4743.
243 J. V. Paulin, S. Bayram, C. F. O. Graeff and C. C. B. Bufon, *ACS Appl. Bio Mater.*, 2023, **6**, 3633–3637.
244 M. d'Ischia, A. Napolitano, A. Pezzella, P. Meredith and M. J. Buehler, *Angew. Chem., Int. Ed.*, 2020, **59**, 11196–11205.
245 A. B. Mostert, *Polymers*, 2021, **13**, 1670.
246 M. Schubert, G. Panzarasa and I. Burgert, *Chem. Rev.*, 2023, **123**, 1889–1924.
247 M. Dadkhah and M. Messori, *Mater. Today Sustain.*, 2024, **27**, 100886.
248 A. Balakrishnan, M. M. Jacob, N. Dayanandan, M. Chinthala, M. Ponnuchamy, D. V. N. Vo, S. Appunni and A. S. Gajendhran, *Mater. Adv.*, 2023, **4**, 5920–5947.
249 H. Furukawa, K. E. Cordova, M. O'Keeffe and O. M. Yaghi, *Science*, 2013, 1230444.
250 S. Begum, Z. Hassan, S. Bräse, C. Wöll and M. Tsotsalas, *Acc. Chem. Res.*, 2019, **52**, 1598–1610.
251 H. Cai, Y. L. Huang and D. Li, *Coord. Chem. Rev.*, 2019, **378**, 207–221.
252 A. Shahzaib, Shaily, L. A. Kamran and N. Nishat, *Mater. Today Chem.*, 2023, **34**, 101781.
253 L. D. Trino, L. G. S. Albano, D. C. Granato, A. G. Santana, D. H. S. De Camargo, C. C. Correa, C. C. Bof Bufon and A. F. Paes Leme, *Chem. Mater.*, 2021, **33**, 1293–1306.
254 M. M. Sabzehmeidani and M. Kazemzad, *Biomater. Res.*, 2023, **27**, 115.
255 A. Wang, M. Walden, R. Ettlinger, F. Kiessling, J. J. Gassensmith, T. Lammers, S. Wuttke and Q. Peña, *Adv. Funct. Mater.*, 2023, 2308589.
256 G. Ding, S. T. Han, C. C. Kuo, V. A. L. Roy and Y. Zhou, *Small Struct.*, 2023, **4**, 2200150.
257 R. K. Parashar, P. Jash, M. Zharnikov and P. C. Mondal, *Angew. Chem., Int. Ed.*, 2024, **63**, e202317413.
258 M. M. Sabzehmeidani, S. Gafari, S. Jamali and M. Kazemzad, *Appl. Mater. Today*, 2024, **38**, 102153.
259 Z. Xu, Y. Li, Y. Xia, C. Shi, S. Chen, C. Ma, C. Zhang and Y. Li, *Adv. Funct. Mater.*, 2024, **34**, 2312658.
260 L. G. S. Albano, T. P. Vello, D. H. S. De Camargo, R. M. L. Da Silva, A. C. M. Padilha, A. Fazzio and C. C. B. Bufon, *Nano Lett.*, 2020, **20**, 1080–1088.
261 D. Xie, G. Gao, B. Tian, Z. Shu, H. Duan, W. W. Zhao, J. He and J. Jiang, *Adv. Mater.*, 2023, **35**, 2212118.
262 M. Giménez-Marqués, T. Hidalgo, C. Serre and P. Horcajada, *Coord. Chem. Rev.*, 2016, **307**, 342–360.
263 P. Bhakat, A. Nigam and S. Jagtap, *Nanotechnol. Environ. Eng.*, 2023, **8**, 815–827.
264 K. Boukayouht, L. Bazzi and S. El Hankari, *Coord. Chem. Rev.*, 2023, **478**, 214986.
265 Z. Ajoyan, P. Marino and A. J. Howarth, *CrystEngComm*, 2018, **20**, 5899–5912.
266 J. Liu, Y. Li and Z. Lou, *Sustainability*, 2022, **14**, 5768.
267 R. S. Forgan, R. A. Smaldone, J. J. Gassensmith, H. Furukawa, D. B. Cordes, Q. Li, C. E. Wilmer, Y. Y. Botros, R. Q. Snurr, A. M. Z. Slawin and J. F. Stoddart, *J. Am. Chem. Soc.*, 2012, **134**, 406–417.
268 M. Salgaonkar, S. S. Nadar and V. K. Rathod, *Int. J. Biol. Macromol.*, 2018, **113**, 464–475.
269 M. Salgaonkar, S. S. Nadar and V. K. Rathod, *J. Environ. Chem. Eng.*, 2019, **7**, 102969.
270 Y. Shu, Y. Meng, M. L. Chen and J. H. Wang, *Chin. Chem. Lett.*, 2015, **26**, 1460–1464.
271 H. M. Pérez-Cejuela, M. Mon, J. Ferrando-Soria, E. Pardo, D. Armentano, E. F. Simó-Alfonso and J. M. Herrero-Martínez, *Microchim. Acta*, 2020, **187**, 201.
272 H. Ma, X. Li, T. Yan, Y. Li, H. Liu, Y. Zhang, D. Wu, B. Du and Q. Wei, *ACS Appl. Mater. Interfaces*, 2016, **8**, 10121–10127.

273 W. Bian, J. Chen, Y. Chen, W. Xu and J. Jia, *Cellulose*, 2021, **28**, 3041–3054.
274 P. P. Sun, Y. M. Li, Y. H. Zhang, H. Shi and F. N. Shi, *J. Alloys Compd.*, 2022, **896**, 163081.
275 S. Yuan, L. Feng, K. Wang, J. Pang, M. Bosch, C. Lollar, Y. Sun, J. Qin, X. Yang, P. Zhang, Q. Wang, L. Zou, Y. Zhang, L. Zhang, Y. Fang, J. Li and H. C. Zhou, *Adv. Mater.*, 2018, **30**, 1704303.
276 L. M. M. Ferro, L. Merces, D. H. S. de Camargo and C. C. Bof Bufon, *Adv. Mater.*, 2021, **33**, 2101518.
277 L. Merces, R. F. de Oliveira and C. C. Bof Bufon, *ACS Appl. Mater. Interfaces*, 2018, **10**, 39168–39176.
278 Y. Kim, A. Chortos, W. Xu, Y. Liu, J. Y. Oh, D. Son, J. Kang, A. M. Foudeh, C. Zhu, Y. Lee, S. Niu, J. Liu, R. Pfattner, Z. Bao and T. W. Lee, *Science*, 2018, **360**, 998–1003.
279 J. Qiu, H. Zhao and Y. Lei, *SmartMat*, 2022, **3**, 447–473.
280 J. Wang, V. K. Bandari, D. Karnaushenko, Y. Li, F. Li, P. Zhang, S. Baunack, D. D. Karnaushenko, C. Becker, M. Faghih, T. Kang, S. Duan, M. Zhu, X. Zhuang, F. Zhu, X. Feng and O. G. Schmidt, *ACS Nano*, 2019, **13**, 8067–8075.
281 C. C. Bof Bufon, J. D. Cojal González, D. J. Thurmer, D. Grimm, M. Bauer and O. G. Schmidt, *Nano Lett.*, 2010, **10**, 2506–2510.
282 R. Sharma, C. C. B. Bufon, D. Grimm, R. Sommer, A. Wollatz, J. Schadewald, D. J. Thurmer, P. F. Siles, M. Bauer and O. G. Schmidt, *Adv. Energy Mater.*, 2014, **4**, 1301631.
283 Y. Lee, V. K. Bandari, Z. Li, M. Medina-Sánchez, M. F. Maitz, D. Karnaushenko, M. V. Tsurkan, D. D. Karnaushenko and O. G. Schmidt, *Nat. Commun.*, 2021, **12**, 4967.
284 L. Chen, H. Bai, Z. Huang and L. Li, *Energy Environ. Sci.*, 2014, **7**, 1750–1759.
285 K. Wang, L. Yao, M. Jahon, J. Liu, M. Gonzalez, P. Liu, V. Leung, X. Zhang and T. N. Ng, *ACS Energy Lett.*, 2020, **5**, 3276–3284.
286 J. Park, S. G. Lee, B. Marelli, M. Lee, T. Kim, H. K. Oh, H. Jeon, F. G. Omenetto and S. Kim, *RSC Adv.*, 2016, **6**, 39330–39334.
287 M. Caillau, P. Crémillieu, E. Laurenceau, Y. Chevolot, J.-L. Leclercq, S. Alekseev, C. Chevalier and T. Delair, *J. Vac. Sci. Technol., B: Nanotechnol. Microelectron.: Mater., Process., Meas., Phenom.*, 2017, **35**, 06GE01.
288 A. Grebenko, A. Bubis, K. Motovilov, V. Dremov, E. Korostylev, I. Kindiak, F. S. Fedorov, S. Luchkin, Y. Zhuikova, A. Trofimenko, G. Filkov, G. Sviridov, A. Ivanov, J. T. Dull, R. Mozhchil, A. Ionov, V. Varlamov, B. P. Rand, V. Podzorov and A. G. Nasibulin, *Adv. Funct. Mater.*, 2021, **31**, 2101533.
289 K. H. Smith, E. T. Montes, M. Poch and A. Mata, *Chem. Soc. Rev.*, 2011, **40**, 4563–4577.
290 A. K. Grebenko, K. A. Motovilov, A. V. Bubis and A. G. Nasibulin, *Small*, 2022, **18**, 2200476.
291 M. Irimia-Vladu, E. D. Głowacki, G. Voss, S. Bauer and N. S. Sariciftci, *Mater. Today*, 2012, **15**, 340–346.
292 N. Thombare, S. Kumar, U. Kumari, P. Sakare, R. K. Yogi, N. Prasad and K. K. Sharma, *Int. J. Biol. Macromol.*, 2022, **215**, 203–223.
293 W. Gao and P. Fatehi, *Can. J. Chem. Eng.*, 2019, **97**, 2827–2842.
294 A. Moreno and M. H. Sipponen, *Acc. Chem. Res.*, 2024, **57**, 1918–1930.
295 N. A. Sagar, S. Pareek, S. Sharma, E. M. Yahia and M. G. Lobo, *Compr. Rev. Food Sci. Food Saf.*, 2018, **17**, 512–531.
296 X. Ma, Z. Jiang, L. Xiang and F. Zhang, *ACS Mater. Lett.*, 2022, **4**, 918–937.